Electronic Theses and Dissertations

2001

Optimization of a Multi-Aixs Electro-Mechanical Scanning System.

Raul Urbina

Follow this and additional works at: http://digitalcommons.library.umaine.edu/etd

Part of the Mechanical Engineering Commons

OPTIMIZATION OF A MULTI-AXIS ELECTRO-

MECHANICAL SCANNING SYSTEM

By

Raul Urbina

B.S. Universidad Panamericana, Mexico, 1997

A THESIS

Submitted in Partial Fulfillment of the

Requirements for the Degree of

Master of Science

(in Mechanical Engineering)

The Graduate School

The University of Maine

May, 2001

Advisory Committee:

Michael Peterson, Assistant Professor of Mechanical Engineering, Advisor

Donald A. Grant, Associate Professor of Mechanical Engineering

Vincent Caccese, Associate Professor of Mechanical Engineering

LIBRARY RIGHTS STATEMENT

In presenting this thesis in partial fulfillment of the requirements for an advanced degree at The University of Maine, I agree that the Library shall make it freely available for inspection. I further agree permission for "fair use" copying of this thesis for scholarly purposes may be granted to the Librarian. It is understood that any copying or publication of this thesis for financial gain shall not be allowed without my written permission.

Signature:

Date: 12/08/2000

OPTIMIZATION OF A MULTI-AXIS ELECTRO-MECHANICAL SCANNING SYSTEM

By Raul Urbina

Thesis Advisor: Dr. Michael Peterson

An Abstract of the Thesis Presented
in Partial Fulfillment of the Requirements for the
Degree of Master of Science
(in Mechanical Engineering)
May, 2001

This thesis presents efforts to enhance the system performance of an ultrasonic scanning machine. New developments in electronics are used to enhance the system performance. This work focuses on optimizing the system repeatability with a robust triggering system for the scanner. The robust triggering system applies new advances in programmable logic devices that make the replacement of complicated digital circuits possible. Modeling of wave propagation through anisotropic media is used to increase the system dynamic range. The model-based gain control compensates for variations in thickness and materials by controlling the excitation pulse amplitude. The automatic gain is implemented using integrated RF signal control components. This thesis demonstrates the use of existing models of elastic waves in a novel application that makes use of modern electronics to control the scanning system.

ACKNOWLEDGMENTS

I would like to thank my adviser, Michael Peterson Ph.D. whose hard work and guidance helped me to produce my thesis. I wish him great success in all his future projects.

I would also like to thank my parents for their support and care and for giving me the opportunity to continue my studies.

Thanks also to my wife, Andrea, for her unconditional love, help and encouragement.

TABLE OF CONTENTS

LIST OF TABLES

LIST OF FIGURES

1. ULTRASONIC SCANNING SYSTEM

1.1 Introduction

More widespread adoption of in-process and in-service inspection is dependent on reduction in cost and an increase in inspection reliability. Automation of the inspection process is key to meeting the required reliability needs and can make inspection a viable alternative for cost sensitive applications. Manual inspection is typically too costly except in critical applications. However, in those applications where cost is less of an issue, reliability of manual inspections is more of a concern. As a result automatic inspection is increasingly becoming the norm in both critical and non-critical applications. Fortunately many Non-Destructive Evaluation processes lend themselves well to automation. In particular, ultrasonic inspection can often be performed for large parts at a reasonable cost using an automatic scanning apparatus.

A number of applications exist in which this situation arises. Ultrasonic scanning of tire casings is one example where a cost-effective system has been successfully produced [1]. A similar example of such a system uses open-architecture robotic crawlers as NDT test platforms [2]. The robotic crawlers have been shown to be well suited to critical applications such as aircraft structures.

Continuous development of these systems is necessary to remain competitive with other methods of detecting defects and to make them adaptable for other applications. This work describes the approach used to optimize the non-destructive testing system for tires. The inspection of a curved airfoil is shown as an alternative application for this type of NDE system.

This thesis contains the efforts to enhance the performance of an electromechanical system through new advances in technology. The work done focuses on the areas of system repeatability and system dynamic range. The ultrasonic scanning system currently used has two areas that required improvement. The triggering for the data acquisition card is unreliable. In addition, the geometry of the part to be scanned results in a change in amplitude due to difference in incident angles in the reduced-axis scanning method that is used. In this work both issues are addressed. The first step is to develop a robust triggering system for data acquisition. The development of a reliable triggering system is necessary to assure that each scan-line is positioned in the image correctly. The second step focuses on the development of a model gain control to compensate for material thickness variations in a C-scan based ultrasonic inspection machine. A correction factor can then be assigned to each scan-line based on a model of curvature and layer characteristics of the part. The automatic gain control method will replace the need for an operator to manually adjust the gain of the received ultrasonic signal for each line of the image.

The evolutionary development of a triggering circuit for data acquisition in the ultrasonic scanning system is described in the next chapter. The design minimizes the effects of electromagnetic noise in the digital signals from an encoder. The design solves

problems with unreliable triggering that arise during circumferential scanning of tires. In this approach it is critical that each rotation of the tire be perfectly aligned. Section 3 describes the implementation of a model-based gain control using matrix propagation methods to compute theoretical transmission coefficients. The control is intended to provide correction coefficients for a reduced-axis scanning system. The method is applicable for scanning complex parts of known contour and thickness. Alternatively either thickness or geometry may be inferred if the material properties are known with some degree of accuracy. Section 4 presents the conclusions and contains suggested future applications and areas for study.

1.2 System Configuration

The system that is considered in this work is a large area inspection system that inspects curved composite structures for defects (Fig. 1). This system is described in a paper published on the general system design [1]. The system is used to detect defects that may make a tire unsuitable for retreading or that may compromise the integrity of curved composite panels in critical applications. For these inspection applications a system was designed that uses one of several possible point defect sensor technologies: ultrasonic sensors. Ultrasonic sensors are desirable because of their ability to penetrate an opaque material. A three-axis scanning system is used for detecting defects of interest. The design for the sensor allows the scanning of a complete tire in less than 7 min, with inspection resolution of 3 or 1.5mm that is determined by the system step size. This corresponds to as many as two hundred fifty thousand points in the ultrasonic image.
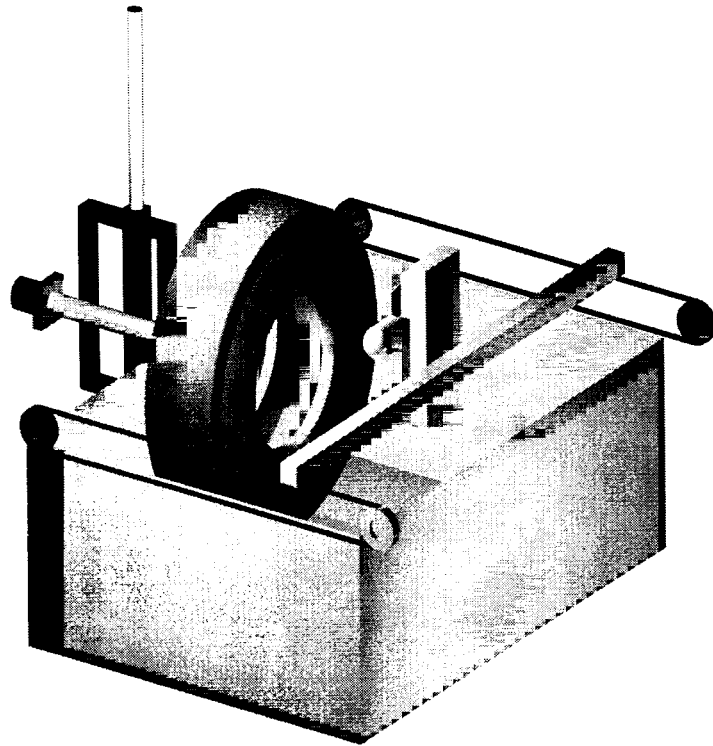
Figure 1: Tank and drive setup of the Ultrasonic Inspection Machine

The system design uses a PC for motion control and high-speed large-data-set data acquisition system. The required data throughput is achieved by relying on a number of embedded subsystems. The overall system is divided in two main parts, a central controller and an immersion, scanning tank. The central controller contains the PC with embedded subsystems. The system uses an Intel architecture to control embedded processors for motion control and data acquisition. A serial line embedded processor controller governs the rotational velocity of the tire during scanning.

Motion control makes use of an embedded motion controller (Parker Compumotor-AT6400 four-axis controller). The motion control card uses the Motorola 68000 processor that is programmable with a motion control language that includes control of the I/O on the motor board. The data acquisition uses an additional embedded

4

processor to avoid interrupt latency in the data acquisition. The controllers are also used to control relays that operate at 24V to switch between pairs of transmitting and receiving transducers.

2. EVOLUTIONARY DEVELOPMENT OF A ROBUST COUNTER CIRCUIT FOR DATA ACQUISITION

2.1 Introduction

A large number of data acquisition tasks continue to require external circuitry for triggering and reset functions. While this need has become less pronounced when using newer high-speed data acquisition boards, the option of simplifying control and off-loading tasks from the data acquisition processor has merit. One application where this type of circuit is commonly used is in point-to-point non-destructive imaging. Imaging methods such as ultrasonic scanning (or c-scan) and microwave methods typically require that a probe be passed across the part or in other pattern with data acquired at each point. Continuous scanning sometimes depends simply on maintaining the speed of the scanning head carefully. However, it is preferable that the motion axis be connected to an encoder that generates trigger interrupts for the data acquisition system. Using this approach the data can be reliably acquired at incremental positions regardless of slight speed variation in the motor system. This approach has led to high-speed low-cost scanning systems for ultrasonic and other applications [1]. Similar issues exist when

using line scan cameras on production lines or any cases where synchronization of motion and data acquisition exists.

In general, the use of an encoder to generate interrupts also requires that a reset be sent periodically to the data acquisition card. While simply counting data points and calculating a reference for a reset is possible, a second pulse interrupt is preferred because of cumulative errors that could result due to errors in the number of points counted. The second interrupt can be sent by the zero or Z-pulse from an encoder. The Z-pulse is generated once per rotation of the encoder (the zero point). In contrast the main pulses (the A or B pulses) may generate 1024 or more pulses per revolution and have a reasonable error rate for triggering the data acquisition card. However the use of the Z-pulse for the reset is preferred to avoid errors. An error occurring every ten or fifteen revolutions can cause significant zero point drift in an image that is assembled from hundreds of line scans. The reset function referenced to the zero degree pulse from the encoder can be used as a reset signal. The scanning system design should be able to function in a manner that random errors do not cause cumulative misalignment of the system or large errors in a single data string.

2.2 Design Requirements

The most significant problem in design and reliability of the overall system has been the required interface electronics [1]. In order to use the commercial motor controller and data acquisition card in this system, interface electronics were designed for a number of the signals. The interface electronics are required for decoding signals received from the encoders that are used to generate interrupts for data acquisition and

7

motion control. The interface electronics are also used for switching signals in several of the auxiliary systems including RF relays used on the ultrasonic lines. All signals used for timing the data acquisition and motion control are either TTL signals or complementary signals , which are decoded in the interface electronics.

Scanning of the tire casing uses a circumferential scanning technique (Fig. 2). An incremental encoder is attached to the rotating shaft and generates pulses based on the angular position (axis z in Fig. 3). The incremental encoder generally generates the three standard signals along with the complementary values. The encoder generates the A and B pulse at a 90° angle difference. These two signals are used to determine the angle of the shaft as well as if it rotates CW or CCW. These two signals can also be used for increasing the resolution of the encoder using a technique called quadrature [3]. The zero pulse (Z-pulse) is also generated for use as a reference point and occurs at each full rotation. For transmitting the signal a complementary signal is used to avoid common-mode noise. The complementary signal, denoted $\overline{A}$, $\overline{B}$ or $\overline{Z}$, has a high value when the A, B or Z signal has a low value and vice-a-versa. The signal will also have better noise immunity performance when the differential signals are used as a twisted-pair of wires. This scheme is familiar in network applications where it is used for enhanced common-mode noise rejection and to generate clean high-speed logic levels in noisy environments [3]. The peak amplitude of the ultrasonic signal is sampled at each of the 2048-encoder pulses during a complete revolution of the tire. Data is acquired based on the generation of an interrupt signal from each pulse of the incremental encoder. After one rotation of the tire, the transducers on the interior of the tire are stepped to a new location and data is
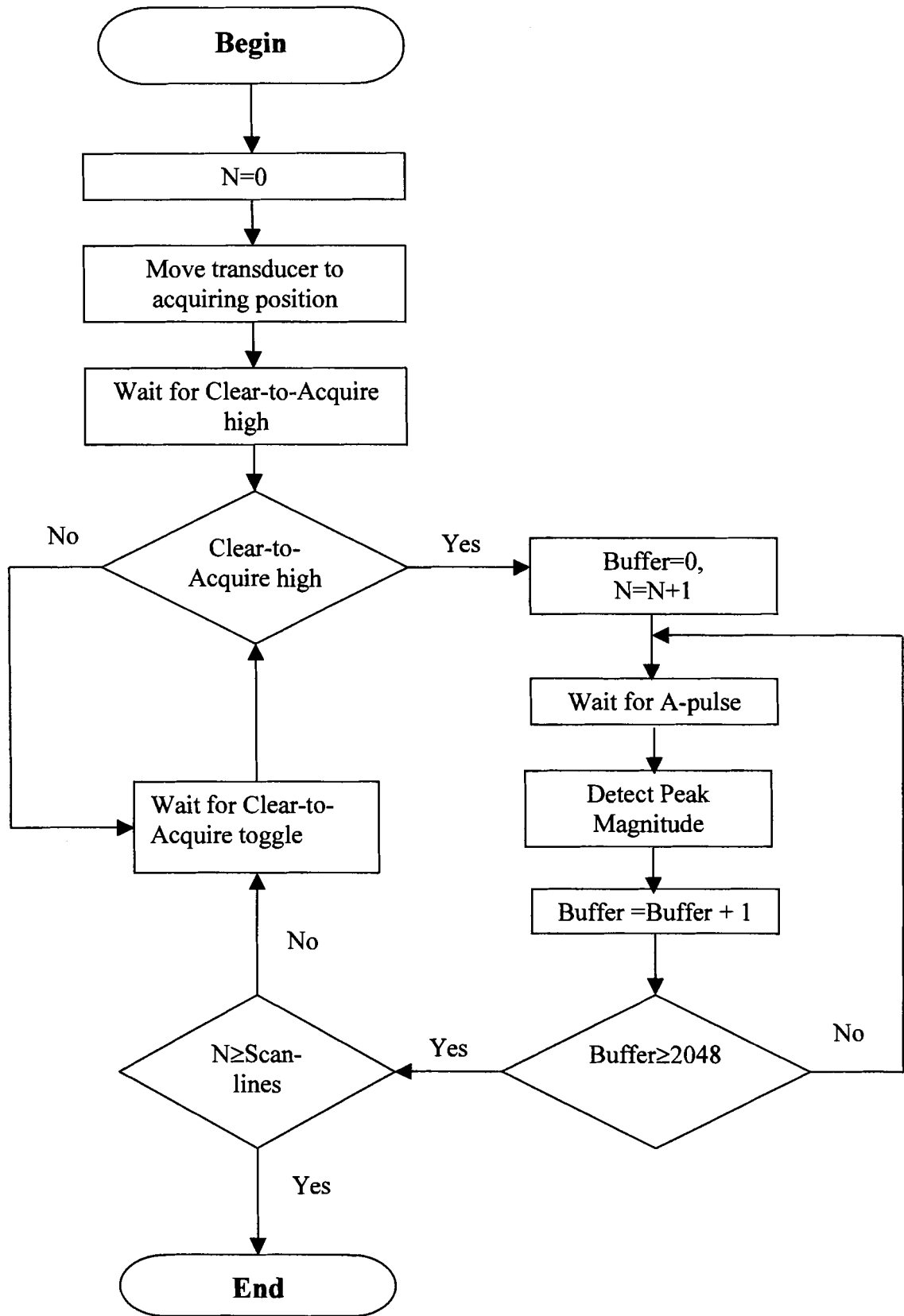
Figure 2: Circumferential scanning flow chart

acquired at the new location [1]. Data is acquired on alternate revolutions of the tire toallow the receiving transducer to move to the new position prior to the start of data acquisition. The logic required is for a Z-pulse to generate a change in state for the data acquisition line, the Z-toggle line. When the Z-toggle line is high and an encoder pulse is generated, data is acquired. After 2048 points a new Z-pulse sets the Z-toggle line low. If either the Z-toggle or the pulse signal is low no data is acquired.
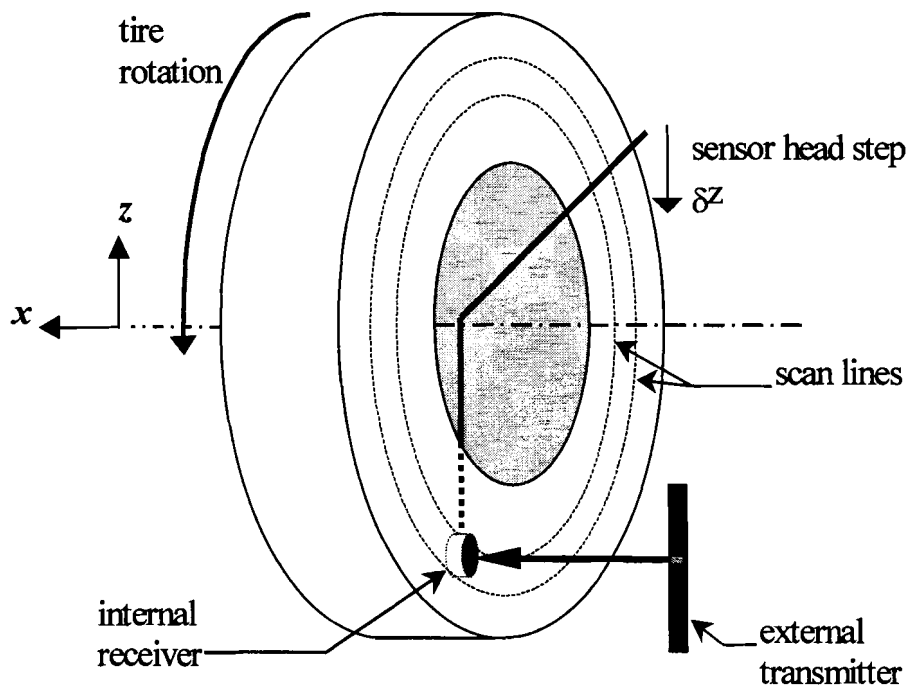
Figure 3: Circumferential scanning showing movement axes

The iterative design for the electronics described is in response to problems that have been encountered when electromagnetic noise generates a false Z-pulse in the system. The false Z-pulse either prematurely indicates the end of the scan resulting in an incomplete line in the final image, or can result in an incorrect starting point for a new

10

scan line. Either case will generate an erroneous image reconstruction and can result in false interpretation of the tire casing condition. Each image consists of at least 400 lines with 2048 points per each line. The reliability required is high since in the 400 lines no errors can be present or the entire image will be defective. Thus, even 1 in 1000 error rate leads to a more than one-third defect-rate for the imaging system. Thus even a low-data acquisition error rate can result in an unacceptable number of bad images.

The design of the required interface electronics began with a simple 7400 series logic electronic circuit [1]. Later developments of the circuit described below use a counter flip-flop to switch the encoder Z-pulse, incorporated a printed circuit board and used application specific integrated circuits. The latest version of the circuit has moved to high reliability programmable logic device. This development has resulted in a low-cost high-reliability circuit.

2.3 Discrete Logic Design

2.3.1 Hand Wired

The initial design of the circuit is shown in Fig. 4. This circuit is based on traditional discrete electronic design. The design relies on 7400 series TTL logic and standard analog circuits with which were hand-wired on a perfboard type of circuit board. The circuit is used to generate the two signals required for the controller, Clear-to-Acquire and Z-toggle. The Clear-to-Acquire signal synchronizes the tire motion to a reference point (Z-pulse) for the acquisition of the first scan line. The Z-toggle signal,

11

Figure 4: Diagram of hand wire synchronization board

which changes its value with Z-pulse, alternates the data acquisition of one scan line with the movement of the transducer (reposition).

To scan the tire using the ultrasonic system, the tire is mounted on the machine. The machine rotates the tire in the Z-axis (shown in Fig. 3). The user enters a command to start scanning. The command to start is passed to the motor controller that generates the Motion-Complete signal when all the movements to position the transducers to the start of the scan are finished. Scanning begins when a Z-pulse is generated by the encoder. The Clear-to-Acquire signal is set to 1 by receipt of a Z-pulse, indicating the start of the data acquisition. The Clear-to-Acquire remains high until the data acquisition signals that the required number of points has been acquired. The scanning program at this point passes control back to the motor control processor that sets the Motion-Complete line to zero. With both Z-toggle and Clear-to-Acquire high the system starts acquiring the data. An A-pulse n the optical increment encoder (BEI Industrial Encoder Division, XH25D-SS-2048-ABCZ-7406R-SM18-S, Goleta CA) generates interrupts used to trigger acquisition of a single point of data. The circumference of the tire is scanned until the machine encounters the second Z-pulse. The system requires that both of the Z-pulse and the A-pulses be reliably received, in order to properly acquire the data received from the two receiving ultrasonic transducers.

The Clear-to-Acquire was initially implemented using a 7474 D-type flip-flop. The preset was set as zero. The output state changes to 1 when a positive-edge of the Z-pulse is received unless the Motion-Complete signal is set to 0. The Z-toggle was implemented using dual JK flip-flops with preset and clear. The initial circuit design used a LM339 quad comparator to decode the complementary signal received from the encoder. The output from the comparator was then sent through an inverter to then

13

sharpen the pulse shape. The complements were generated through additional inverters, although the complements were not used in the design.

The controlling signals for the ultrasonic RF relays and other auxiliary systems such as circulation pumps were switched using NPN Q2N2222 transistors. The signals from the data acquisition digital lines were first inverted and then taken to the base on a transistor. A 24V-power source was then supplied to the collector of the transistor to produce the 24V-output signal used to switch the relays.

2.3.2 Robust PCB

The initial design was sufficiently unreliable that it was completely unacceptable in this application. In particular, the encoder lines were susceptible to electromagnetic noise that generated false Z-pulses. The whole system was also insufficiently isolated from power line noise. It was necessary to improve the reliability of the system for it to be use. The new design that resulted will be referred to as the robust PCB board. To improve the error rate on the encoder lines a specialized integrated circuit was used. The complementary signals generated from the encoder were transmitted through a twisted pair of cables from the encoder to the electronics, a distance of approximately fifty feet. These complementary signals are similar to the RS-485 signals used in communication [4]. Instead of the LM339 comparator and inverter used in the initial design, a Maxim 490 was used to generate the TTL signal from this complementary input. These low-power transceivers for RS-485 and RS-422 communications are employed in harsh environments and have a reduced slew-rate drivers that minimize EMI susceptibility and reduce the reflections that are caused by improperly terminated cables. These chips are designed to allow error-free data transmission up 2.5 Mbps.

14

The 7476 flip-flop was also found to be unreliable. A more effective solution was to use the flip-flop from a 74LS92 divide-by-12 counter. The buffering in the counter increased the reliability of generation of the Z-toggle pulse. In addition to these design-changes a 4-layer commercial printed circuit board (PCB) was designed and professionally made. The use of a PCB significantly decreased the number of failures due to physical connections. This redesign was sufficient to allow the machine to be used for tire casing inspection.

2.4 CPLD Design

2.4.1 Circuit

While the more robust PCB circuit increased the reliability, further improvements were required (Fig. 5). The new design is based on a reduced chip count and better signal isolation. Using a complex programmable logic device (CPLD) and the associated software allows a more complex design to be implemented, while reducing the complexity of the physical design. CPLDs are ICs that contain configurable logic blocks that can be easily programmed using the associated software (Xilinx, Foundation Series, San Jose CA). Unlike circuits built with discrete IC's, it is not necessary to build a separate board for each application. The program can be changed and tested with limited effort. Improvement to the circuit can be implemented without designing a new PCB, as long as the changes are possible within the limitations of the programmable logic device and the connections are accommodated on the original PCB. Issues such as timing delay are also considered automatically without the need to employ additional circuit

simulation software. Finally, due to the reduced chip count, the number of solder connections is decreased.
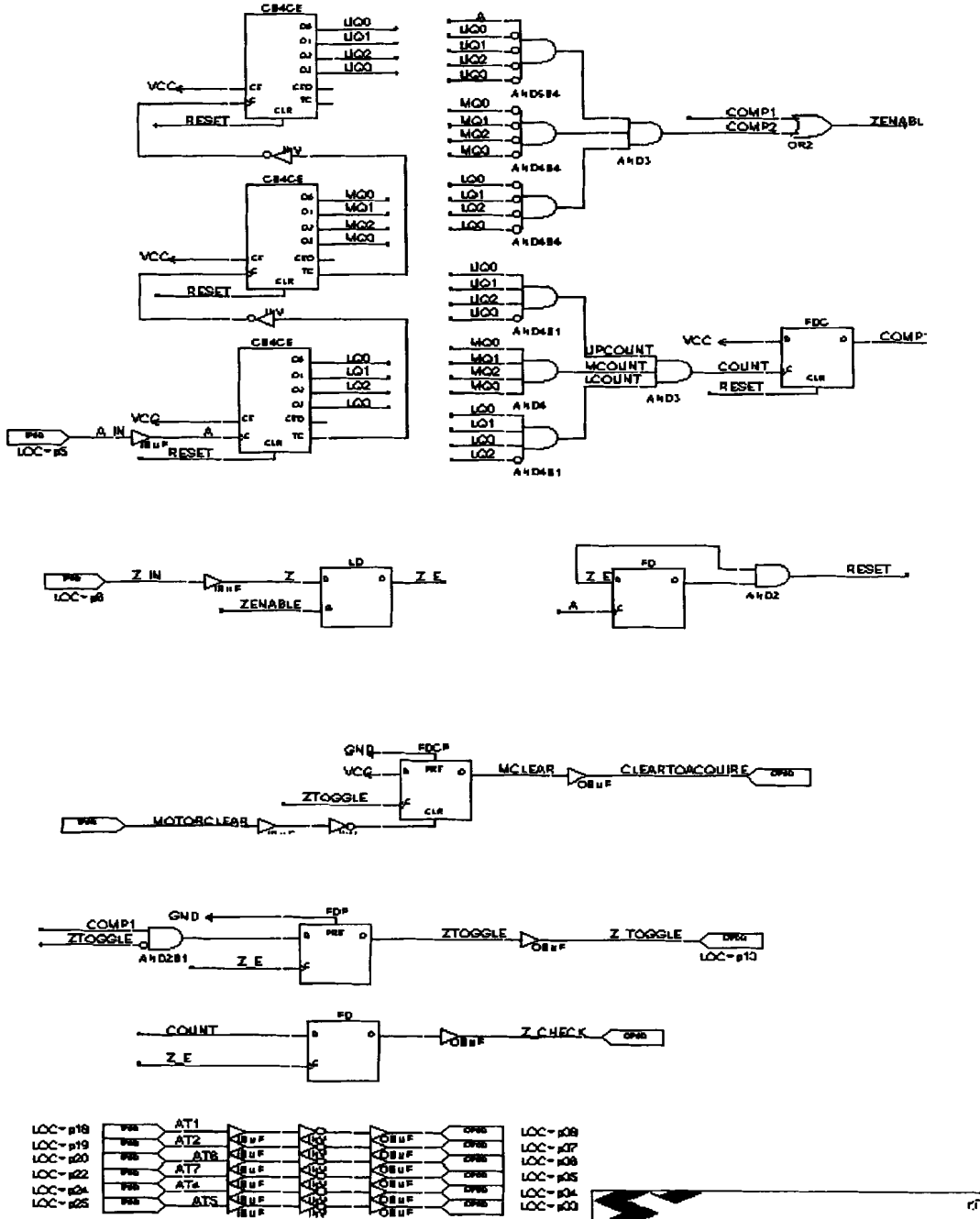
Figure 5: CPLD program for the synchronization board
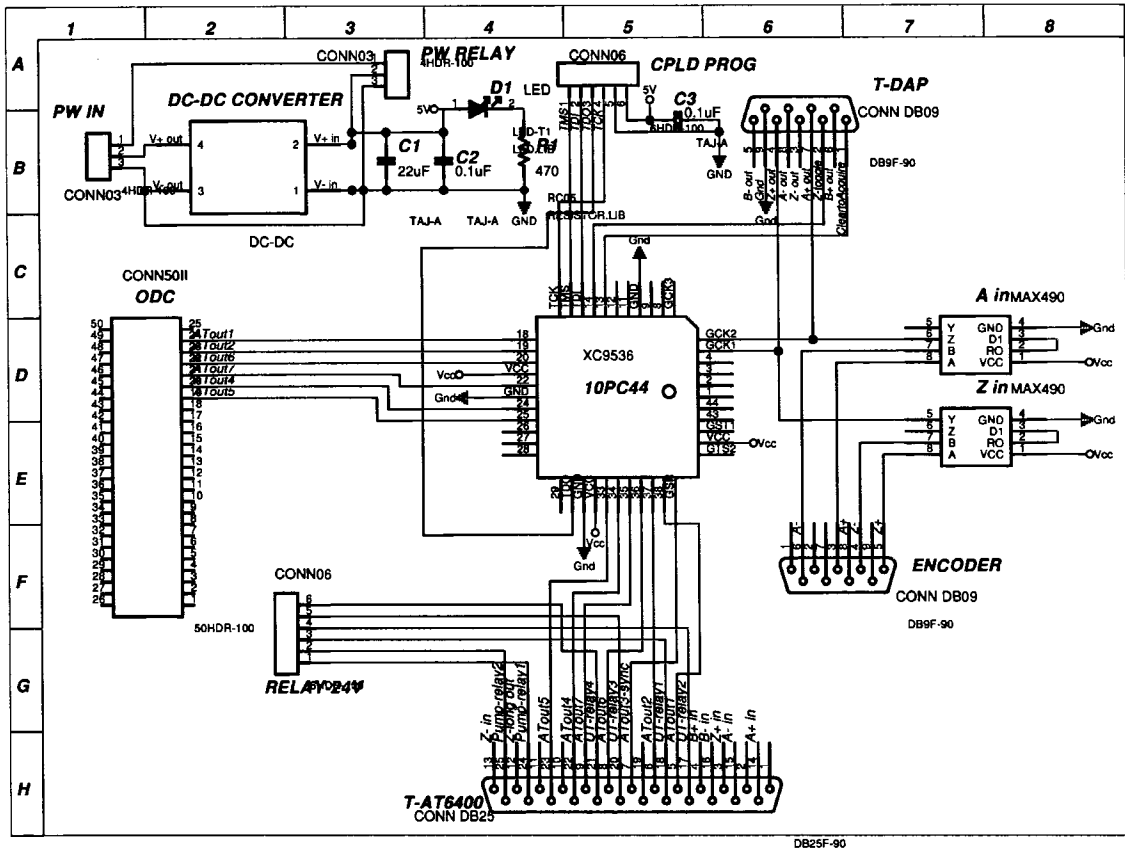
Figure 6: Synchronization Board Diagram using CPLD

As with previous designs, the CPLD based design uses the signal from the A-pulse to generate interrupts for data acquisition (Fig. 6). The complementary encoder signals, transmitted through twisted pairs, are first decoded through Maxim 490 transceivers to maintain resistance to common-mode noise. However, the Z signal is not the only source for the Z-toggle. The Z-pulse is also cross-referenced to a count of A-pulse signals. The A-pulse signals are counted to ensure that approximately 2048 changes of state occur before a Z-signal is acquired. This count indicates one complete rotation of a tire and provides improved confidence that an actual Z-pulse has been

17

received. It was assumed that it was acceptable if a Z-pulse was skipped due to an error in a pulse counting since slower scanning with no errors is acceptable. While the counting of pulses is possible to implement using 7400 series logic, the number of chips would increase significantly and the overall reliability would be likely to decrease.

In addition, complete isolation of all other signal lines was also included in the new design. A DC-DC converter was used on the input power line to maintain a constant voltage level and to provide up to 500VDC of power-line isolation for the CPLD chip and other ICs. The control signals for the relays were also isolated. In the prior design the transistor circuits were prone to failure and did not isolate the channels. The transistors proved to have finite life and required periodic replacement. Output DC modules (Potter & Brumfield, ODCM-5, Peachtree City GA) were used on all of the channels. These modules are used to interface computer-based control systems with external devices and loads such as switches and sensors. The output modules are connected to a 2IO8 mounting board and can switch up to 60 VDC using a 5V logic signal. The modules also provide 4000V of optical isolation to protect the logic circuits.

2.4.2 Program

Unlike the 7400 series logic, the CPLD must be programmed. Software is used to provide several features that are suitable for customizing the CPLD chip for a desired application. The two modes available for programming the CPLD are a schematic programming mode and an advanced-programming mode [5]. The schematic mode is the simpler design tool and it is complemented by a logic simulator. In this interface, standard components such as encoder, flip-flops, multiplexers, etc. are chosen from a menu and the operation of the CPLD chip is simulated. The advanced mode (HDL,

hardware description language) requires the programmer to directly implement the logic tree. More complicated logic such as loops can be implemented directly using the advanced mode since it is like a procedural computer language. HDL-based system designs are most useful in large projects, where several designers or teams of designers are working concurrently. The schematic mode was better suited to the simple replacement of the 7400 series logic and to reduce the programming complexity. The schematic mode also allows the changing signals in all the extensions of the program to be altered simultaneously.

The CPLD also has two operational modes, low power and high speed. In order to reduce power consumption and the need for heat dissipation in the system the low power mode of the chip was used [6]. The high-speed operation was not required since the CPLD in low power mode has stated switching speeds of less than 43ns. The other settings for programming the chip were left in the default mode.

The new circuit requires two signals, the A-pulse and Z-pulse, in order to generate the Z-toggle. The value is set with the Z-pulse, and then any changes in the Z-pulse are disabled until a set number of counts of the A-pulse were reached. The Z-toggle signal then changes with the next Z-pulse. An enable signal was used to allow a change in the value of the Z-toggle signal. It was also discovered, not surprisingly, that significant noise is present in the A signal. When the counter reaches a minimum of 2044 A-pulses, a high value is set enable signal (Fig. 7). A high enable signal (ZENABLE) allows the change of state for the Z-toggle with the next Z-pulse.
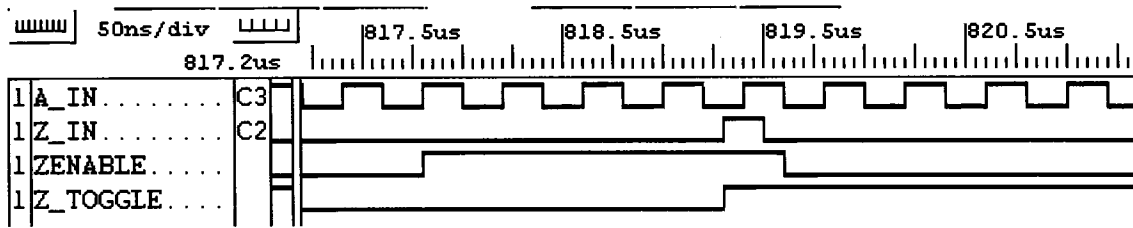
Figure 7: Logic simulation for Z toggle signal using Foundation Software

In the programming logic, the Z-toggle signal was preset to zero. A full rotation of the tire is required prior to an enable signal to be set to 1. The full rotation is required to make sure that the start is at a Z-pulse and not at an alias. When the Z-toggle has a 1 value the Clear-to-Acquire signal can only be set to 1, if the input signal for the line is 1. The Clear-to-Acquire indicates that all of the motor motion generated by the motor control processor and indicates all motion is complete. If the motion is not complete, the value remains at 0. The motor controller enables motion after a single line of data is acquired.

An initial reset on the counter was implemented to avoid metastability problems. Metastability in digital systems can occur when data input to a flip-flop is asynchronous to the clock. It appears as unreliable changes of state, flip-flop output oscillations or no change of state due to an input. Most metastability difficulties are usually caused by setup violations. The reset was generated to take advantage of the fact that the A-pulse is in a different phase that the Z-pulse. The system was designed so that it allowed the change of the Z-toggle to occur before generating the reset signal.

20

2.5 Results

Improved reliability of the system will result in an increase in the number of scan lines that can be acquired without an error. Image-reconstruction is improved by error reduction as well as increasing machine throughput. Since a single defective scan line acquisition results in a defective image, the reliability required of the interface electronics is high. By reducing the number of bad scans, the amount of time necessary for inspection of the tire casing is reduced.

The original 7400 series based circuit resulted in approximately one fault in every fifty lines when operated in an industrial setting. As a result, only one image reconstruction in several trials was successful. This was not a workable solution and immediate improvements were needed in the system. The more robust PCB board circuit resulted in approximately one fault in every seven hundred to one thousand scan-lines (Fig. 8). This result gives approximately one unsuccessful image reconstruction in every three, four hundred line images. While the Maxim 490 transceivers and the flip-flop from a counter resulted in a significant improvement over the first design, the proper functioning of the machine requires a more reliable circuit. The new design that uses the CPLD reduces the number of errors in the data acquisition so that in testing no errors were observed (Fig. 9). The very low error rate circuit has significantly enhanced the reliability of the inspection process.
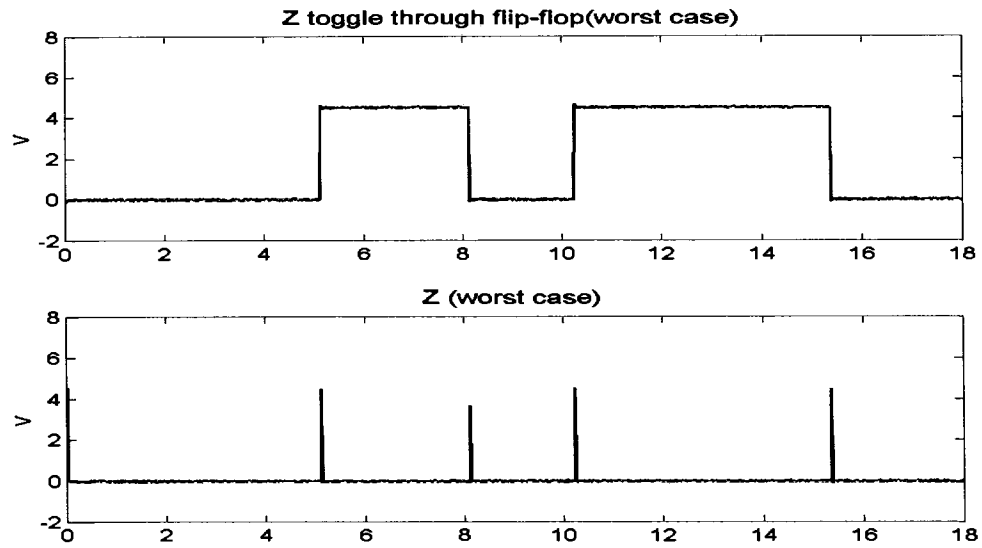
Figure 8: Z toggle signal with electromagnetic noise using flip-flop
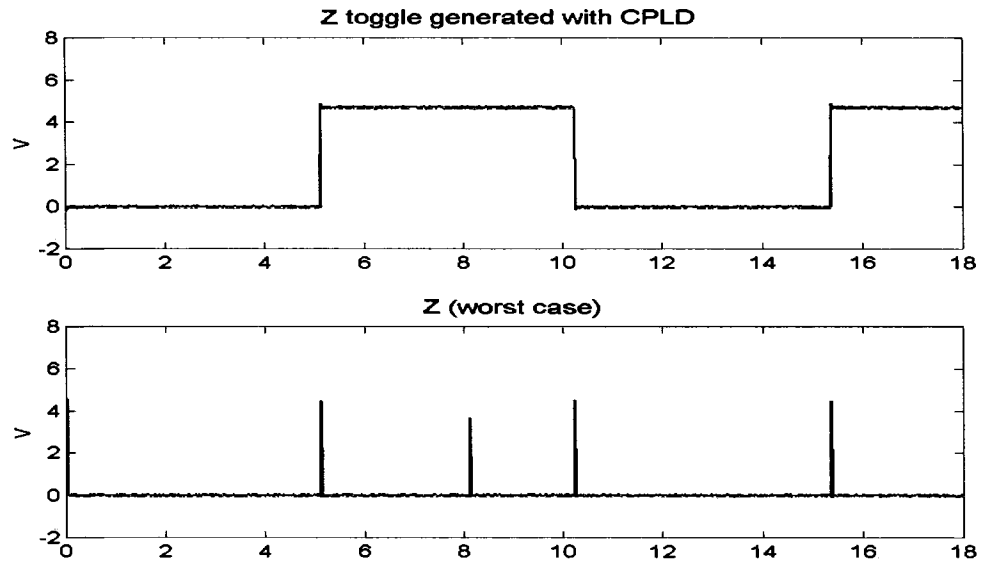
Figure 9: Z toggle signal using CPLD board

While the target of one error in every hundred images has not been shown to be met, it appears that the error rate from the interface electronics is now quite low. The improved machine is becoming more efficient overall as the error rate is reduced. Long

term durability of the circuit is also expected to improve due to reduced number of connections. The original design required 5 chips and 264 solder connections. The robust PCB design had 6 chips and 212 solder connections. The current design only requires 3 chips and 102 solder connections. This reduction in number of connections is also expected to significantly improve the long-term reliability of the circuit.

Subsequent to the improved reliability of the system steps can be made to find a correction factor for the scan line. The correction factor can be used to implement the automatic gain control. This will greatly enhance the efficiency of the inspection process.

3. AUTOMATIC GAIN CORRECTION FOR REDUCED

AXIS SCANNING

Submitted for publication in Experimental Mechanics, SEM, Bethel, CT

3.1 Introduction

One of the challenges facing automatic scanning systems is that in many cases the part geometry may not be known precisely. In other applications the geometry may be sufficiently complex that it requires a scanning system with a large number of degrees of freedom to follow the part contours during inspection. For ultrasonic inspection, refraction of the wave front occurs across the oblique incident wave interface between the coupling fluid and the part. However, in cases where the acoustic impedance of the coupling fluid and the part is closely marched, the refracted angle of the wave is small. For many important aerospace applications water coupling provides a sufficiently close impedance match that reasonably large incident angles can be accommodated. If the acoustic impedance is reasonably well matched, a relatively complex part may be scanned without precisely following the part contours. It is possible in those cases to scan a complex part and to be less exact in following the profile. Alternatively, a reduced number of degrees of freedom may be used in the scanning system. Thus a close acoustic impedance match between the part and the coupling fluid can make reduced axis

scanning possible for higher efficiency and lower cost [1]. The reduction in the number of degrees of freedom in a scanning system can also result in a more reliable system. However, while reasonable ultrasonic signal amplitude may be obtained when scanning a part using this approach, the resulting attenuation of the wave may be sufficiently high that amplitude correction of the received signal may be required. The use of non-normal incidence scanning is not currently widespread. However, the use of reduced axis scanning has become more reasonable as significant computational resources have become available at minimal cost while the cost of scanning hardware has remained relatively high. An ultrasonic system can thus be produced that does not precisely follow the part contours if an amplitude correction factor is applied to the signal to correct for the contour. Amplitude correction is important since without the correction it is possible to have both false positives and false negatives (detecting a flaw when none exists) depending on the part curvature.

Thus an analytical method or efficient numerical model is needed that can be used to correct the received signal to account for refraction and loss of amplitude which occurs due to the curvature. The model should be able to accommodate composite parts since many of the most important applications are in aerospace. It is reasonable for the material to be modeled as layered. For these applications, matrix propagator methods are well suited for the creation of a model that will allow the effect of amplitude variation on the received signal to be corrected for non-normal wave incidence. Matrix propagator models allow, in general, multi-layer anisotropic materials to be considered a multi-layer model. The magnitude of the received signal can be adjusted so that it is consistent regardless of the angle of incidence. This modeling approach is well established in the

literature. Application of this technique to the inspection of a part with a complex curvature is considered within the context of use on a reduced axis scanning system [7]. Some modifications to the manners in which theoretical results have been reported in the past is required. In the past calculations were normally performed at a single frequency. The results are reported in terms of the transmission coefficient versus angle for a single frequency. This is reasonable from a theoretical perspective, however for experimental applications single frequency excitation is rarely used. The traditional method of ultrasonic imaging is to extract the peak value from a broadband transmitted signal using an analog circuit [8]. While some more modern systems perform the same task using a digital circuitry [1] the principle of operation is similar. As a result, the transmission coefficient curve of interest is the peak of a broadband transmitted signal versus angle. The result is much less general since it is dependent on the bandwidth of the transducer used for the application. However, the curve does represent the type of signal that is normally used in practice. In particular the use of a broadband signal effectively averages the theoretical signal removing sharp peaks in the transmission coefficients. This curve is then directly comparable to the experimental data as well as being useful for gain correction. A further important result is that the curves may be used to design a transducer configuration. In this way reasonable results may be obtained even if the part geometry is not known precisely.

3.2 Theoretical Formulation

Automatic gain correction is primarily intended for the calculation of transmission coefficients for orthotropic or even isotropic layered materials at arbitrary incident angles. By necessity though, lower effective material symmetries result. When the orthotropic case is considered for a non-normal angle of incidence in a direction other than an axis of material symmetry, a lower effective material symmetry results. In this case the propagation of the shear waves and longitudinal wave are coupled. Thus, the formulation will consider more general material symmetry in order to treat the orthotropic case for a general angle of incidence. The transfer matrix method is then applied to the calculation of transmission coefficients for use in the automatic gain correction algorithm. Because variation in amplitude in a point to point scan is of interest, only relative amplitude is needed. Since the absolute variation in amplitude is not of primary interest in the model, elastic material description can be used. However, visco-elastic effects should also be considered if large thickness variation is present. Otherwise, the material attenuation from visco-elastic material properties is not expected to have significant variation between points.

3.2.1 Wave Propagation in an Elastic-Composite Material Layer Immersed in Water

In the matrix transfer method, general solution equations and boundary conditions are expressed in a simplified matrix form and, the transmission coefficients are obtained by matrix operations [9]. Generally, the solutions are derived from the equations of motion, the constitutive relations and the strain-displacement relations. The general form of calculated matrix is expressed in term of stresses and displacements as a 6th order

matrix. In the more general form, the propagation of the three waves, two shear waves and one longitudinal wave, are coupled.
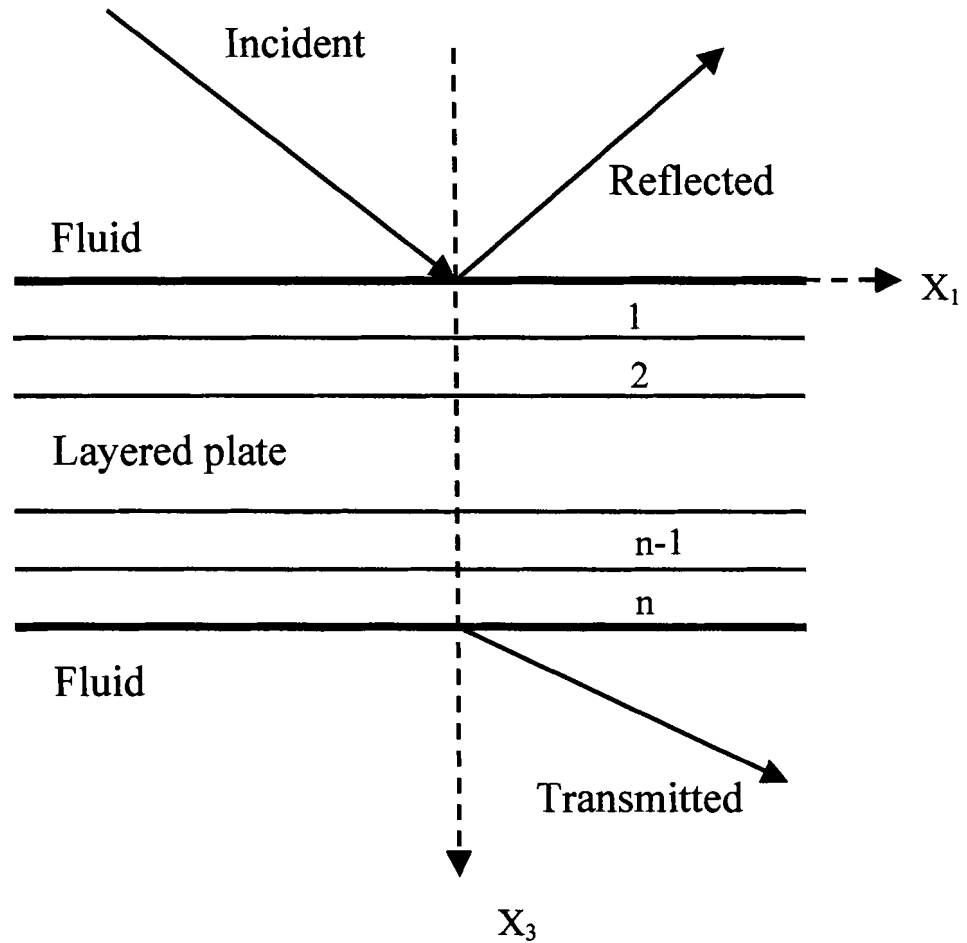
Figure 10: A laminated composite plate immersed in water

For the configuration shown in Figure 10, the layers are assumed to be a series of orthotropic plates with the sample immersed in water. When an incident beam is propagated in the fiber direction, the horizontally polarized shear (SH) wave propagating in the $x_1 \square x_3$ plane at an arbitrary angle from the normal is uncoupled. The SH wave is

independent of a vertical quasi-shear (SV) wave and a quasi-longitudinal (L) wave. Only a vertically polarized quasi-shear wave and a quasi-longitudinal wave are produced because when an incident longitudinal wave is propagated in the water fluid coupling layer. Thus in the orthotropic case only the coupled vertically polarized shear wave and longitudinal wave are considered. In general when the orthotropic material is combined with an incident beam plane in the fiber direction, the 6th order transfer matrix degenerates into a 4th order transfer matrix which includes the 2 coupled waves. The transmission coefficient may be expressed as [10]:

$$T = \frac{2N}{(M_{21} + QM_{22}) + Q(M_{11} + M_{12})}$$ (3.1)

where:

$$\begin{bmatrix} M_{11} & M_{12} \\ M_{21} & M_{22} \end{bmatrix} = \begin{bmatrix} A_{21} & A_{22} & A_{23} \\ A_{31} & A_{32} & A_{33} \end{bmatrix} \cdot \begin{bmatrix} -A_{42} & -A_{43} \\ A_{41} & 0 \\ 0 & A_{41} \end{bmatrix}$$ (3.2)

$$N = A_{41}$$ (3.3)

$$Q = \rho_w c^2 / \alpha_w$$ (3.4)

$$\alpha_w{}^2 = (c/c_w)^2 - 1$$ .... (3.5)

29

where $[A]$ is the global transfer matrix, ρ_w is the water density and c is called the common phase velocity. The common phase velocity is equal to $c_i/\sin(\theta_i)$ where c_i is the velocity in layer i and $\sin(\theta_i)$ is the propagation angle in layer i.

However, when the propagation vector of the incident beam is no longer oriented in the direction of one of the planes of material symmetry, the coupling of the waves increases. The propagation of the wave in an orthotropic material becomes effectively a monoclinic propagation problem. The horizontally polarized quasi-shear wave (SH), the vertically polarized quasi-shear wave (SV) and the quasi-longitudinal wave (L) are all coupled. A 6th order matrix expression is used in the calculation of the transmission coefficient. The form of equation (3.1) remains the same, but, M_{11}, M_{12}, M_{21}, M_{22} become 3rd order determinants that depend on the material properties and the orientation of the sample [11]. The global transfer matrix determinants are then of the form:

$$M_{11} = \det\begin{vmatrix} A_{31} & A_{32} & A_{33} \\ A_{51} & A_{52} & A_{53} \\ A_{61} & A_{62} & A_{63} \end{vmatrix}, \qquad M_{12} = \det\begin{vmatrix} A_{31} & A_{32} & A_{34} \\ A_{51} & A_{52} & A_{54} \\ A_{61} & A_{62} & A_{64} \end{vmatrix} \qquad (3.6)$$

$$M_{21} = \det\begin{vmatrix} A_{41} & A_{42} & A_{43} \\ A_{51} & A_{52} & A_{53} \\ A_{61} & A_{62} & A_{63} \end{vmatrix}, \qquad M_{22} = \det\begin{vmatrix} A_{41} & A_{42} & A_{44} \\ A_{51} & A_{52} & A_{54} \\ A_{61} & A_{62} & A_{64} \end{vmatrix} \qquad (3.7)$$

$$N = \det\begin{vmatrix} A_{51} & A_{52} \\ A_{61} & A_{62} \end{vmatrix} \qquad (3.8)$$

30

Although equation (3.1) becomes slightly more computationally expensive, the basic problem is fundamentally the same for the monoclinic case. Both cases are important to consider, however, since numerical instabilities are encountered when the monoclinic case is used for orthotropic symmetry. As with other similar formulations, stability should be considered as well as the efficiency of the algorithm for real time implementation [12].

3.2.2 Implementation and Verification

The program developed in this case is intended to serve as a correction factor for a reduced axis scanning system. It is thus necessary to either perform real-time computations or else a use data table to look-up values found from using matrix propagation methods. In this case the computational load is sufficiently low that real time calculations are possible. Figure 11 shows a flow chart for the calculation of the transmission coefficients. The program was implemented in Matlab and run on a low-end personal computer. The time needed to run the program is sufficiently small that on-the-fly correction of the signal amplitude can be made for most scanning systems when using a compiled version of the program.

The inputs to the model include the incident angles and the material properties of each layer of the material. The single layer properties are then assembled into the laminate within the program. The tensor material properties in the program are calculated from the engineering constants by standard relations [13]. Nine-independent elastic stiffness material parameters are required for orthotropic materials. In addition to the elastic property data, the input data for the calculations includes material density, fiber lay-up direction angles and the thickness of each of the lamina.

31

```
                    ┌─────────────┐
                    │    Start    │
                    └──────┬──────┘
                           │
                           ▼
        ╱────────────────────────────────────────╲
       ╱ Input: Stiffness matrices, densities,     ╲
      ╱  thickness', Orientation of layers,          ╲
     ╱   Incident angles, Transducer signal           ╲
      ╲  waveform, Frequencies, water phase          ╱
       ╲ velocity and water density. n=0.           ╱
        ╲────────────────────────────────────────╱
                           │
            ┌──────────────┼──────────────┐
            │              ▼              
            │       ┌─────────────┐
            │       │    n=n+1    │
            │       └──────┬──────┘
            │              ▼
            │    ┌───────────────────┐
            │    │ Calculate Xₙ matrix│
            │    └─────────┬─────────┘
            │              ▼
            │  ┌──────────────────────────┐
            │  │ Calculate Aₙ transfer matrix│
            │  └────────────┬─────────────┘
            │               ▼
         no │         ╱──────────╲
            └────────┤  n ≥ No. of │
                      ╲  layers    ╱
                       ╲──────────╱
                           │ yes
                           ▼
           ┌──────────────────────────────┐
           │ Calculate A global transfer matrix│
           └───────────────┬──────────────┘
                           ▼
           ┌──────────────────────────────┐
           │ Calculate transmission coefficients│
           └───────────────┬──────────────┘
                           ▼
           ┌──────────────────────────────┐
           │ Filter transmission coefficients│
           └───────────────┬──────────────┘
                           ▼
           ┌──────────────────────────────┐
           │   Calculate peak magnitude    │
           └───────────────┬──────────────┘
                           ▼
            ╱────────────────────────────╲
           ╱   Display transmission        ╲
          ╱    coefficients and            ╱
           ╲   calculated signal          ╱
            ╲────────────────────────────╱
                           │
                           ▼
                    ┌─────────────┐
                    │    Stop     │
                    └─────────────┘
```
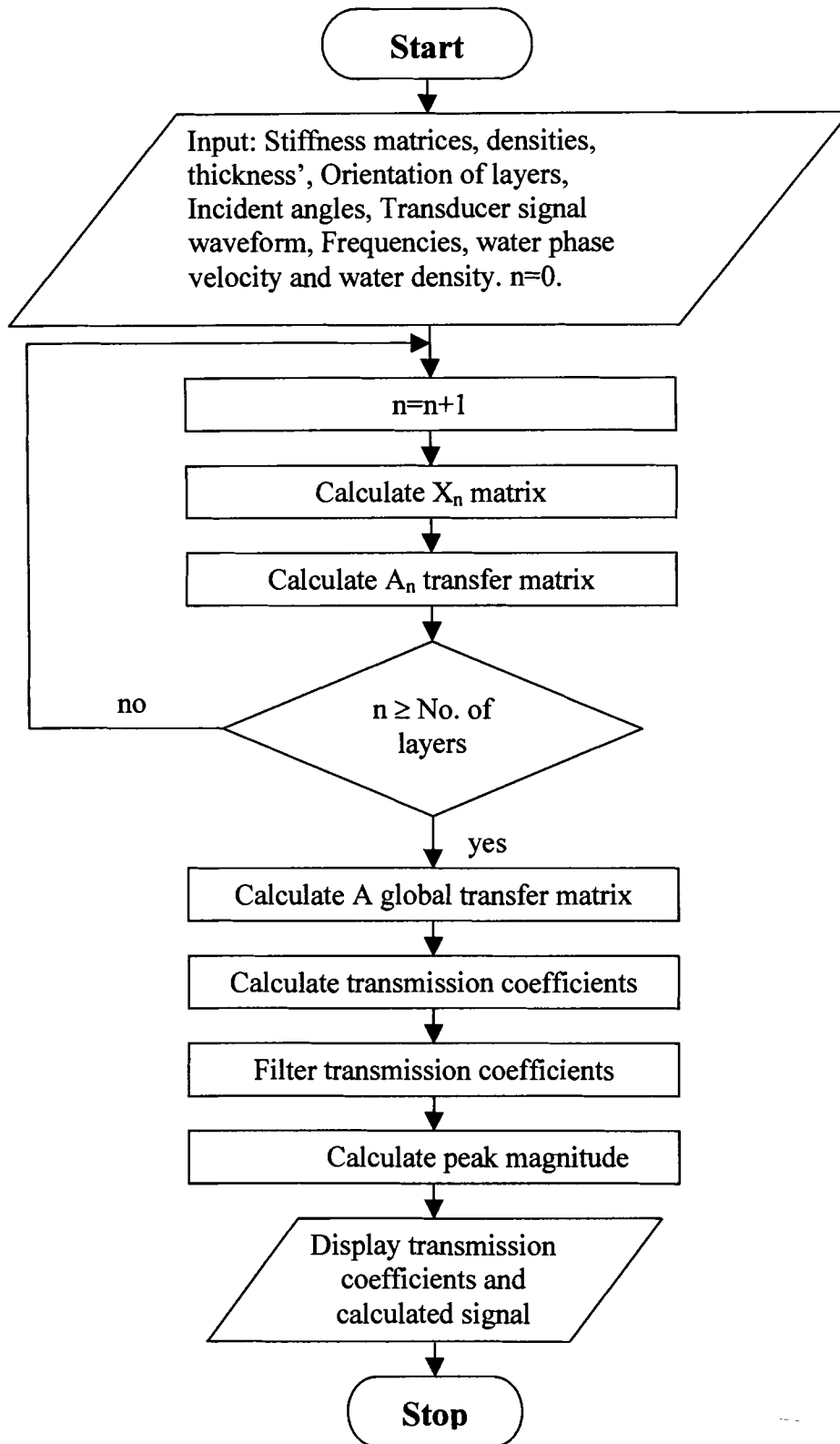
Figure 11: Flow chart for the calculation of transmission coefficients through a
multi-layered solid

32

To test the current implementation, Figure 12 shows a comparison between the points on a frequency versus transmission coefficient calculation, which is compared, to previous work by Chimenti and Nayfeh [14]. The figure shows reflection coefficients for a $[0_2, 90_2]_s$ laminate with an incident angle of 16 degree and with the fiber direction of the uppermost ply in the incident plane. The fiber direction in the uppermost ply is perpendicular to the incident plane. Further details of the configuration used by Chimenti and Nayfeh are shown in the paper [14]. This comparison is useful to verify implementation of the code.
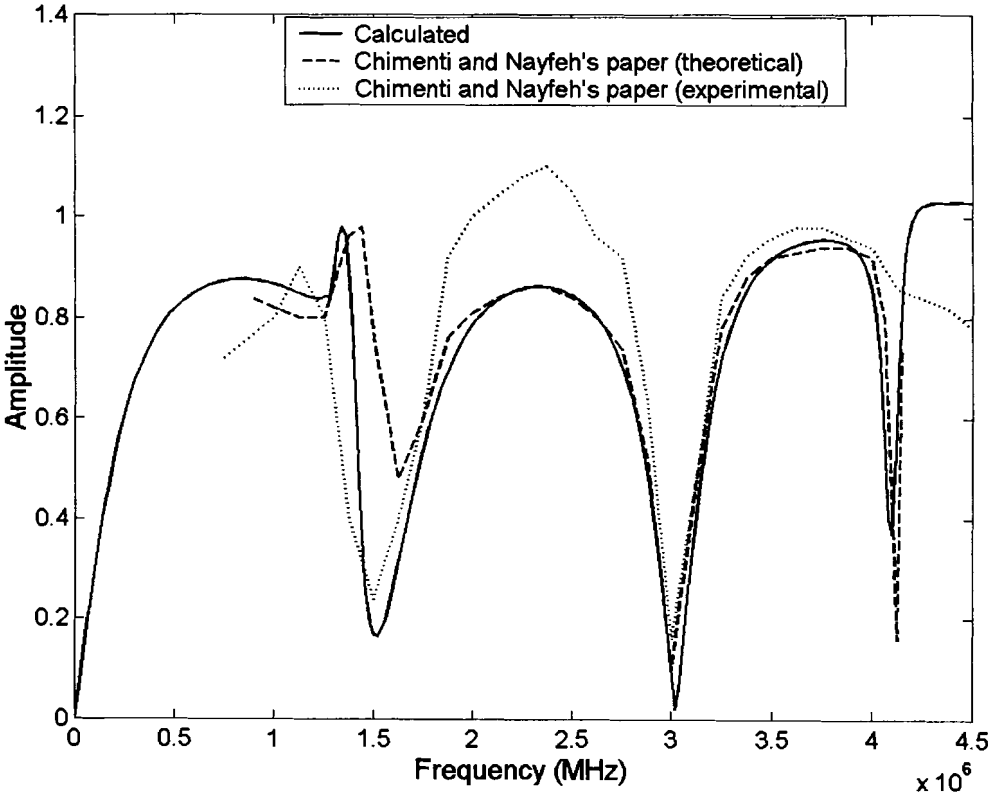

Figure 12: Comparison of calculated results to previous paper
(Reference Chimenti and Nayfeh, 1990)

3.3 Experiments

3.3.1 Experimental Setup

Initial testing of the algorithm for gain correction applications is based on flat samples. Three samples of carbon fiber reinforced epoxy were fabricated from CYCOM 950-1 fiber and T650-35 epoxy prepeg. Lay-up sequences of $[0]_{4T}$, $[0,90]_s$ and $[90,0]_s$ were used. The modulus of the material was obtained from a mechanical test of single lamina and verified using a technique based on similitude to the coefficient of thermal expansion [15]. The elastic tensor obtained for the material is shown in table 2. Measured sample thickness varied between the three samples, $[0]_{4T}$, $[0,90]_s$ and $[90,0]_s$ with a thickness of 0.508 mm, 0.635 mm and 0.520 mm, respectively. The density of the material was approximately 1.5 g/cm^3.

Table 1   Young's modulus and shear modulus for each layer of carbon fiber epoxy materials

E_1(Gpa)	E_2(GPa)	E_3(GPa)	G_{12}(Gpa)	G_{13}(GPa)	G_{23}(GPa)
137.3	8.4	8.4	4.36	4.36	2.27

Table 2.   Elastic constants [C] (GPa) and density (kg/m^3) for each layer of carbon fiber epoxy materials

i	C_{1i}	C_{2i}	C_{3i}	C_{4i}	C_{5i}	C_{6i}
1	141.3	5.90	5.90	0.	0.	0.
2	5.90	11.47	5.88	0.	0.	0.
3	5.90	5.88	11.47	0.	0.	0.
4	0.	0.	0.	2.27	0.	0.
5	0.	0.	0.	0.	4.36	0.
6	0.	0.	0.	0.	0.	4.36
Density ρ	1500.					

Digital Storage Oscilloscope TDS 520

Pulser / Receiver

CH 1 CH 2 AUX 1 AUX 2

T/R   R

Trigger

U. Signal

GPIB communication link
To IEEE STD 488 Port (osc.)

Personal Computer

Specimen

Transducer
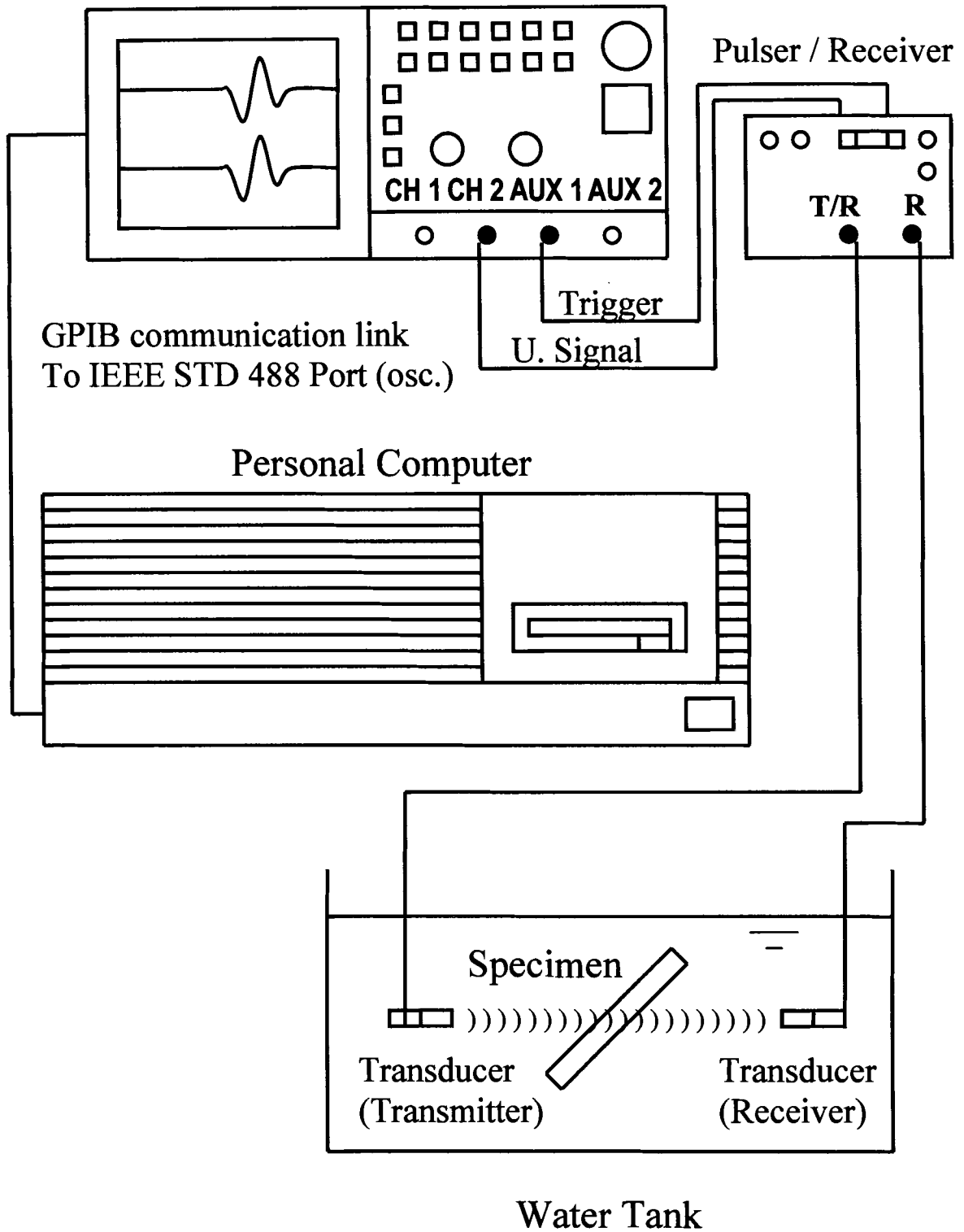(Transmitter)

Transducer
(Receiver)

Water Tank

Figure 13: System configuration for the experimental data acquisition

The experimental set-up for the ultrasonic tests is shown in Figure 13. The experimental equipment includes an ultrasonic pulser-receiver, a digitizing oscilloscope, two piezoelectric transducers, a motion control system and a personal computer. The system is configured so that the angle of the sample between the two transducers can be adjusted precisely using an optical positioner. The signals are acquired at each angle for transmission through the sample. An additional signal is acquired without the sample as a reference signal to describe the propagation through water. The transmission coefficients for each sample at different angles may be found by the deconvolution of the reference signal from the received signal [16]. The experiments are useful as further verification of the model and also provide information about the sample material properties.

All of the experiments were carried out in this water immersion system using the through-transmission configuration. The matched pair of piezoelectric transducers used have a nominal center frequency of 2.25 MHz. A focused transmitter and a flat receiver with a 12-mm element diameter were used. The useable bandwidth of the transducers was chosen to be the frequency ranges over which the magnitude of the spectrum was greater than 75 percent of the peak value. The transducers were excited using a short duration pulse from the pulser-receiver 5052PR (Panametrics, Waltham MA). The signal was oversampled, 250 Msamples/sec. using a digital storage oscilloscope (Tektronix TDS 520A) and the signal was transferred to a personal computer using a general-purpose interface bus connection (GPIB).

The results of lay-up sequences of $[0]_{4T}$, $[0, 90]_s$ and $[90, 0]_s$ are shown in Figures 14, 15 and 16 respectively. The thickness used for each of the lamina in these cases were assumed to be 0.127mm, 0.130 mm, 0.159 mm which are consistent with the

36

nominal thickness of the lamina used in the experimental results below. All laminas are assumed to have the same thickness for each sample.
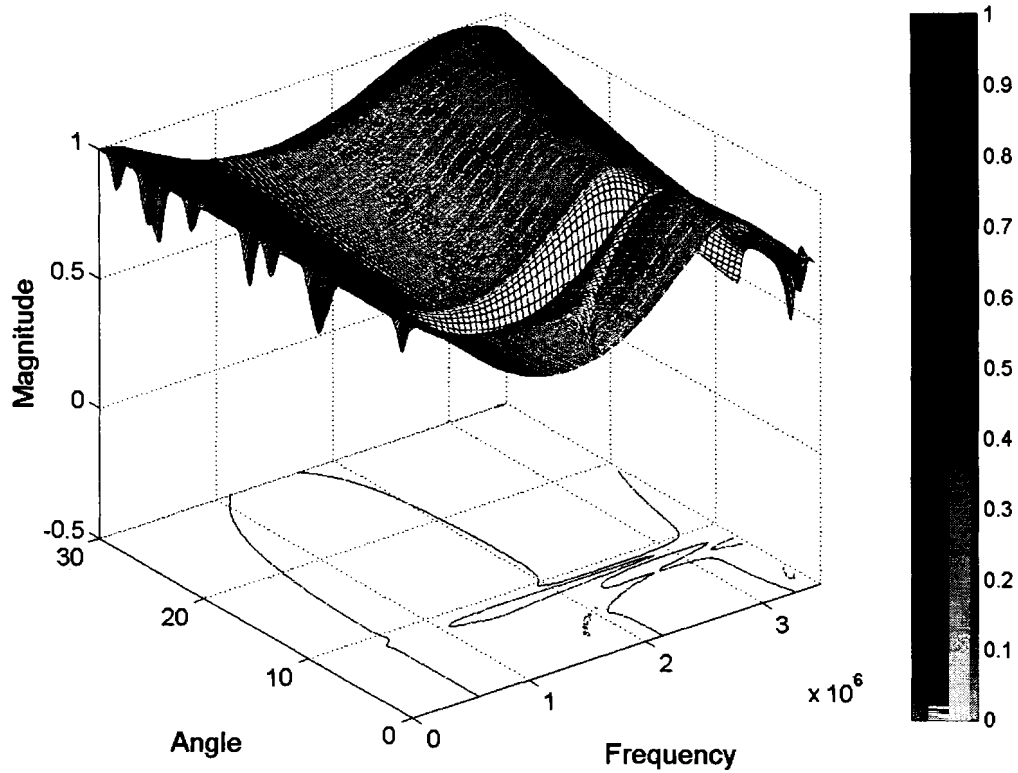

Figure 14: Calculated curves of transmission coefficient versus frequency for the carbon fiber composite of $[0]_{4T}$ lay up, at incident angle 00 to 30
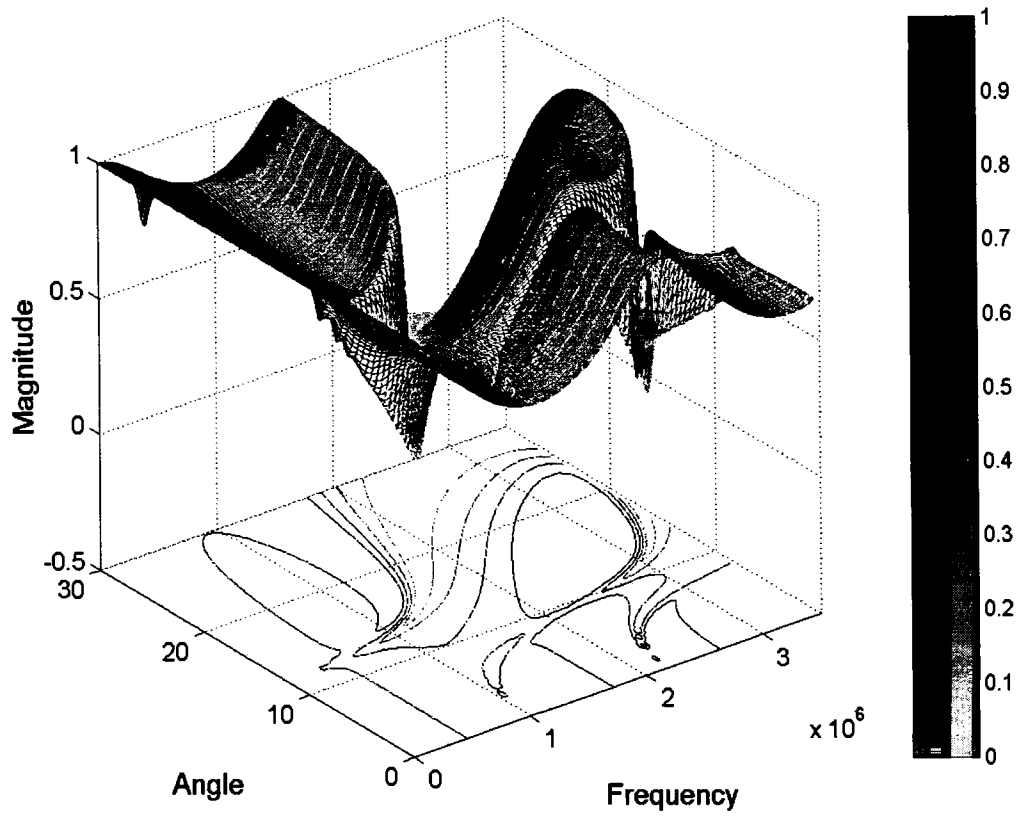
Figure 15: Calculated curves of transmission coefficient versus frequency for the carbon fiber composite of $[0, 90]_s$ lay up, at incident angle 00 to 30
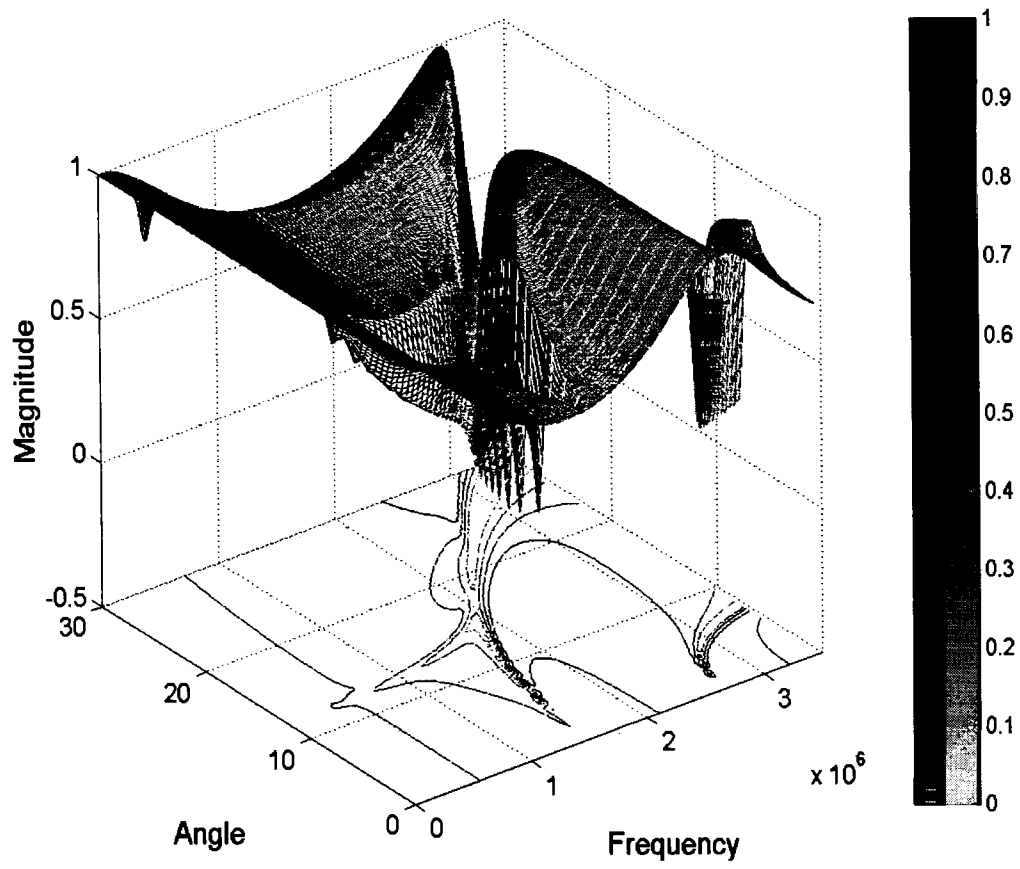
Figure 16: Calculated curves of transmission coefficient versus frequency for the carbon fiber composite of $[90, 0]_s$ lay up, at incident angle 00 to 30

3.3.2 Results

Figures 14, 15 and 16 show the simultaneous dependence on angle and frequency for the transmission coefficient of the 3 lay-up sequences considered. These figures show the relatively smooth response with respect to frequency for most angles and frequencies. For some angles and frequencies abrupt discontinuities exist in the data that are related to numerical instabilities in the system [12]. The effect of these instabilities is reduced with an increase in the number of frequencies used. In practice, more than one angle of incidence results when a signal is generated by a transducer with a finite aperture. A finite impulse response filter was used to model this effect. A Gaussian distribution was used to construct the coefficients of the filter with σ equal to 0.5 degrees. This is intended as a simplified version of the finite aperture integral used by other researchers [10]. The instabilities in the model are removed by averaging, thus leaving a response that is closer to experimental results while maintaining the simplicity of the model. Good agreement was found in it in the range from 0 to 15 degrees incident angles in all the three samples. It appeared that some inconsistency in the phase prediction may occur in a perfectly elastic model. However since the practical problem requires only the use of the peak amplitude this effect is minimized. Phase angle has not in the past been considered in experimental comparisons [7].

In order to provide data that can be used in the experimental amplitude correction algorithm, it is necessary to convolve the transducer response with the transmission coefficient at each angle. The transducer response is approximated by transmitting a pulse through water in the absence of the sample. The reconstructed time signal is created by performing an inverse Fourier transform on the product of the convolution

between the approximate transducer response and the transmission coefficient. The reconstructed frequency domain signal is found from:

$$A(\omega) = T(\omega)W(\omega) \tag{3.9}$$

where $A(\omega)$ is the reconstructed the transmitted signal, $T(\omega)$ is calculated transmission coefficient and $W(\omega)$ is the incident signal that is approximated by the water path signal. In the time domain the convolution integral path signal becomes for discrete data set of length N:

$$a(t) = \sum_{\tau=1}^{N} w(\tau) \cdot t(\tau - t) \tag{3.10}$$

where a(t) is the reconstructed transmitted signal, t(t) and w(t) are the calculated transmission coefficient and the water path signal respectively in the time domain.

The additional processing steps were implemented in a Matlab program to obtain the transmitted signal for different angles using the equation (3.10). For reduced axis scanning the change in the peak magnitude of the transmitted signal at different incident angles is required. The ultrasonic image is simply an assembly of the peak amplitude values at different points. The amplitude correction only requires that the change in the peak due to non-normal incidence that results from the part curvature be obtained. The peaks of the reconstructed signals were calculated at a range of incident angles (0, 02, ...

30) and compared with the experimentally obtained peaks values. The results are shown

in figures 17, 18, 19 for the $[0,90]_s$, $[0]_{4T}$ and $[90,0]_s$ carbon fiber laminates, respectively.

Figure 17: Comparison of theoretical and experimental results for transmission
coefficient of peak of the broadband signal versus incident angle for $[0, 90]_s$
carbon fiber composite
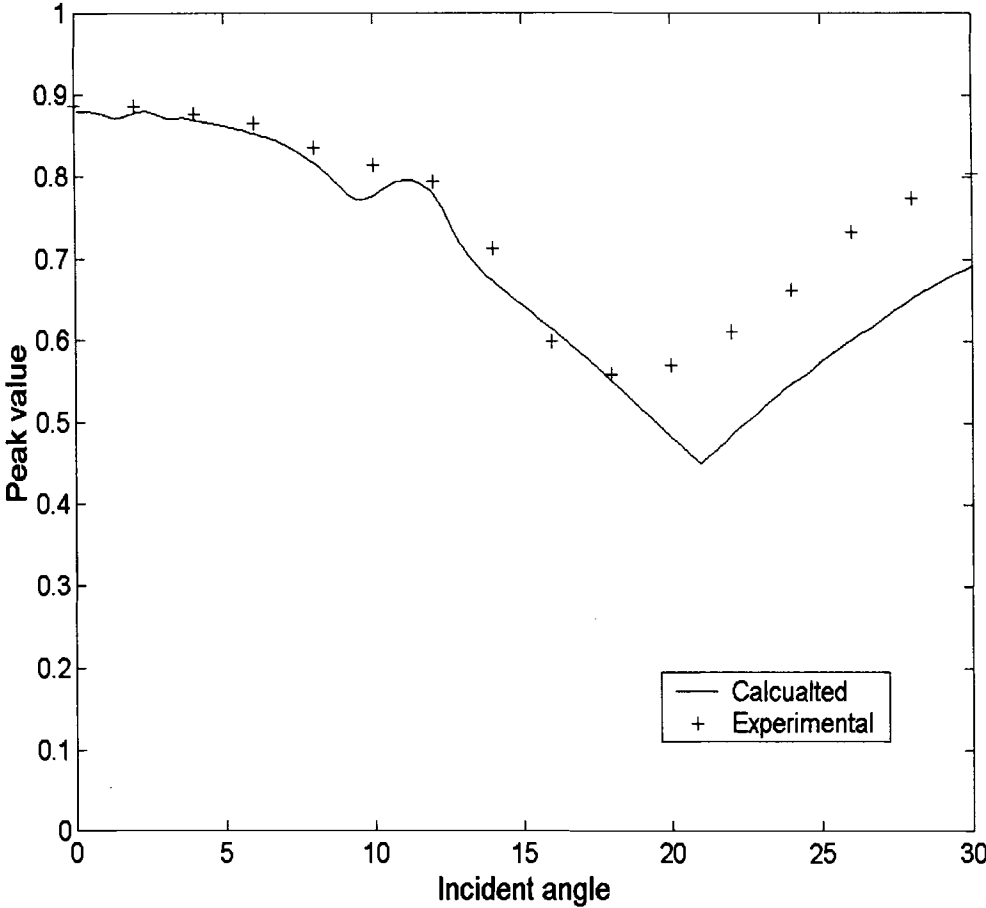
Figure 18: Comparison of theoretical and experimental results for transmission coefficient of peak of the broadband signal versus incident angle for $[0]_{4T}$ carbon fiber composite
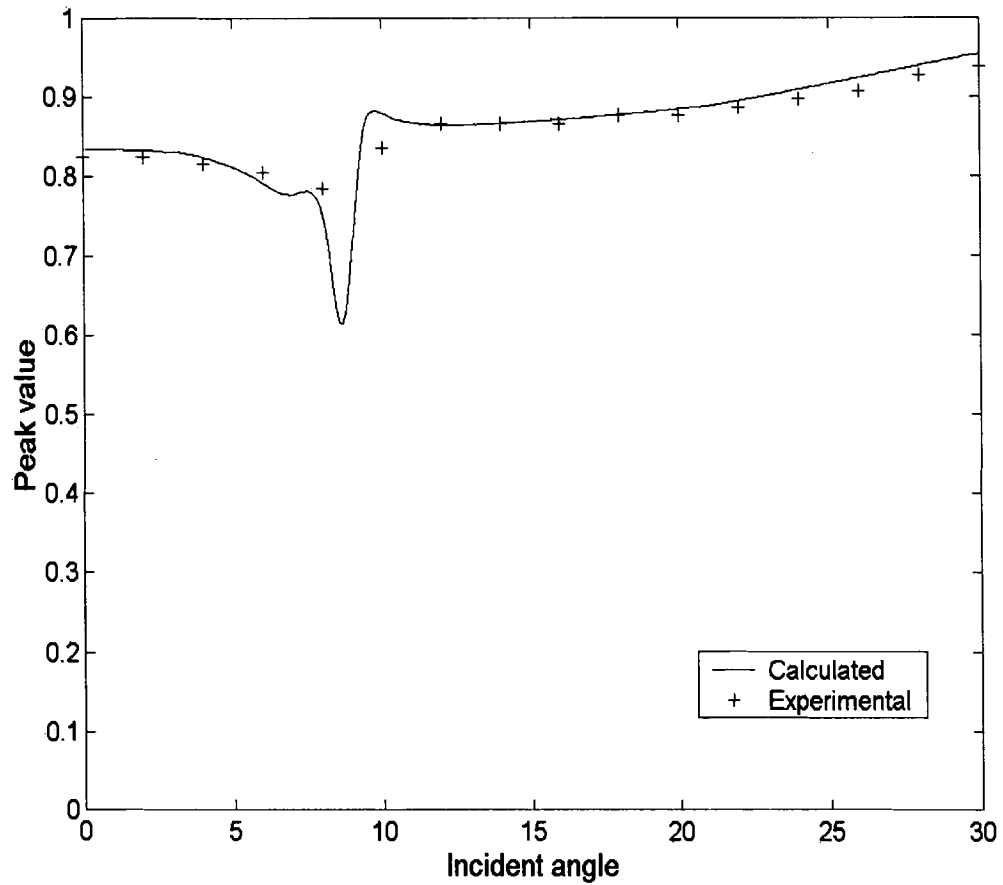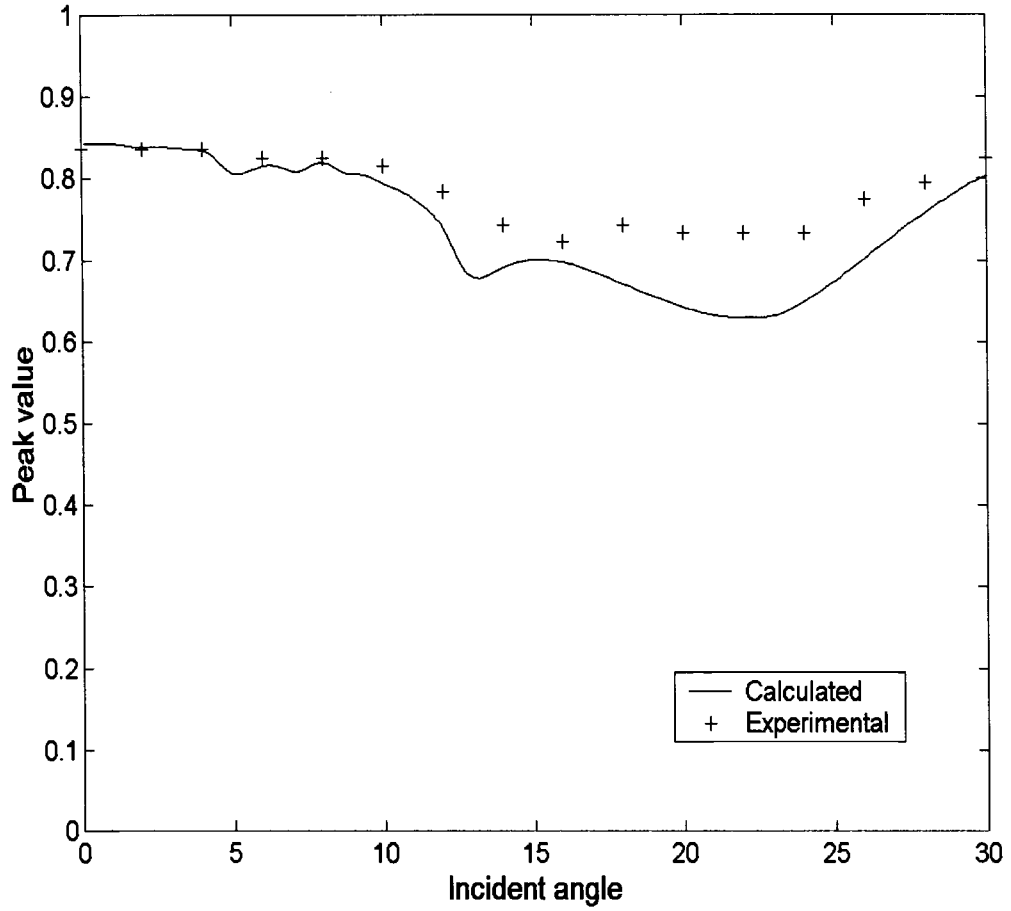
Figure 19: Comparison of theoretical and experimental results for transmission coefficient of peak of the broadband signal versus incident angle for $[90, 0]_s$ carbon fiber composite

3.4 Proposed Configuration to Scan an Airfoil

Based on the results for a flat coupon at different angles, the method is applied to a simple composite structure. Figure 20 shows an airfoil used to mount a video system under a research vessel [17]. The actual structure is a complex asymmetric lay-up, which is use to couple torsion and bending in the strut. For the preliminary configuration a simple $[0,90]_s$ lay-up similar to one of the test coupons is used. Due to environmental concerns with the carbon in seawater, periodic structural inspections are planned. Figure 21 shows the planned configuration of the ultrasonic inspection transducers for one-half of the strut configuration. Two paintbrush transducers are used to insonify the exterior of the half section of the strut as in other reduced-axis scanning systems [1]. The simplified scanning system involves moving the two receiving transducers in a straight line on the concave side of the airfoil. After each linear motion of the transducer the airfoil is then indexed in the x-direction. The lines are then assembled into an image after the amplitude of each signal is corrected. Figure 22 shows the range of angles for the two-transducer configuration. At each angle the theoretical amplitude is found and compared to the signal propagated through a composite specimen at the same angle. The comparison is shown in Figure 23.
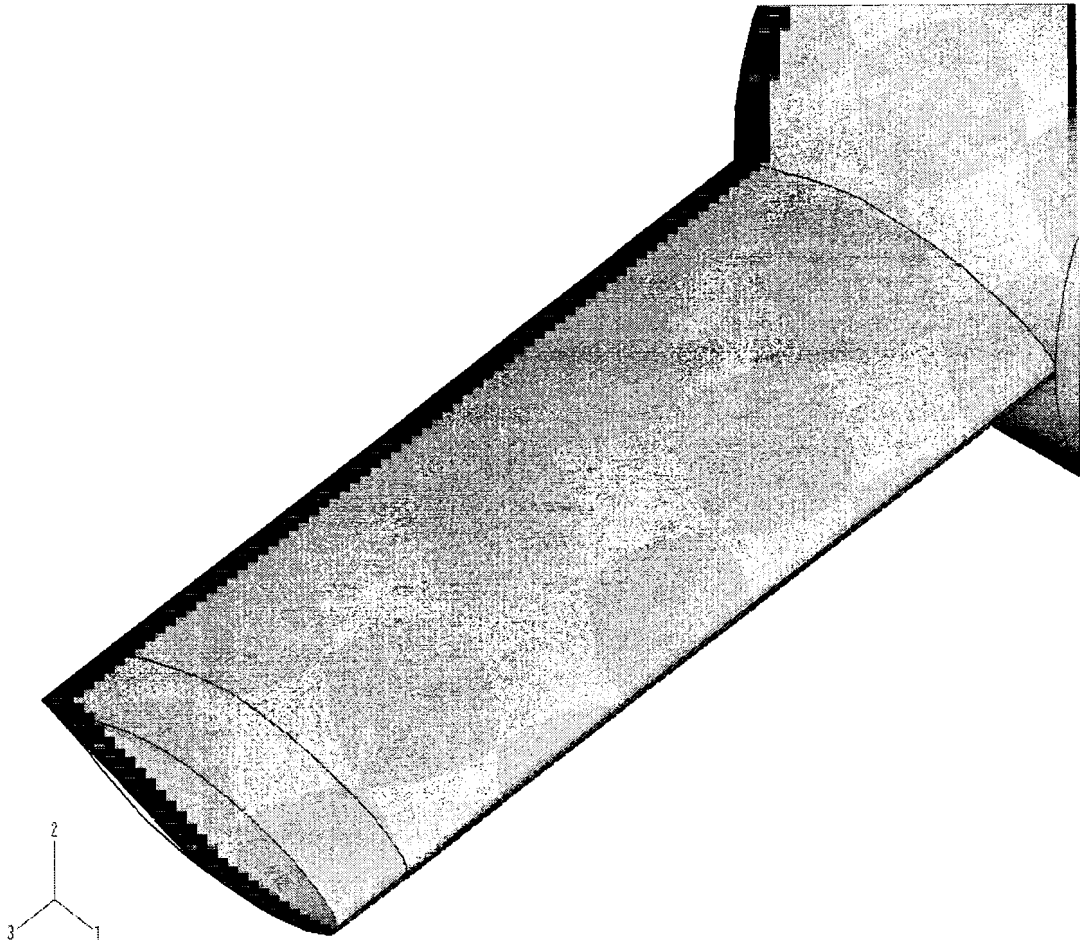
Figure 20: Carbon fiber airfoil design for underwater video system
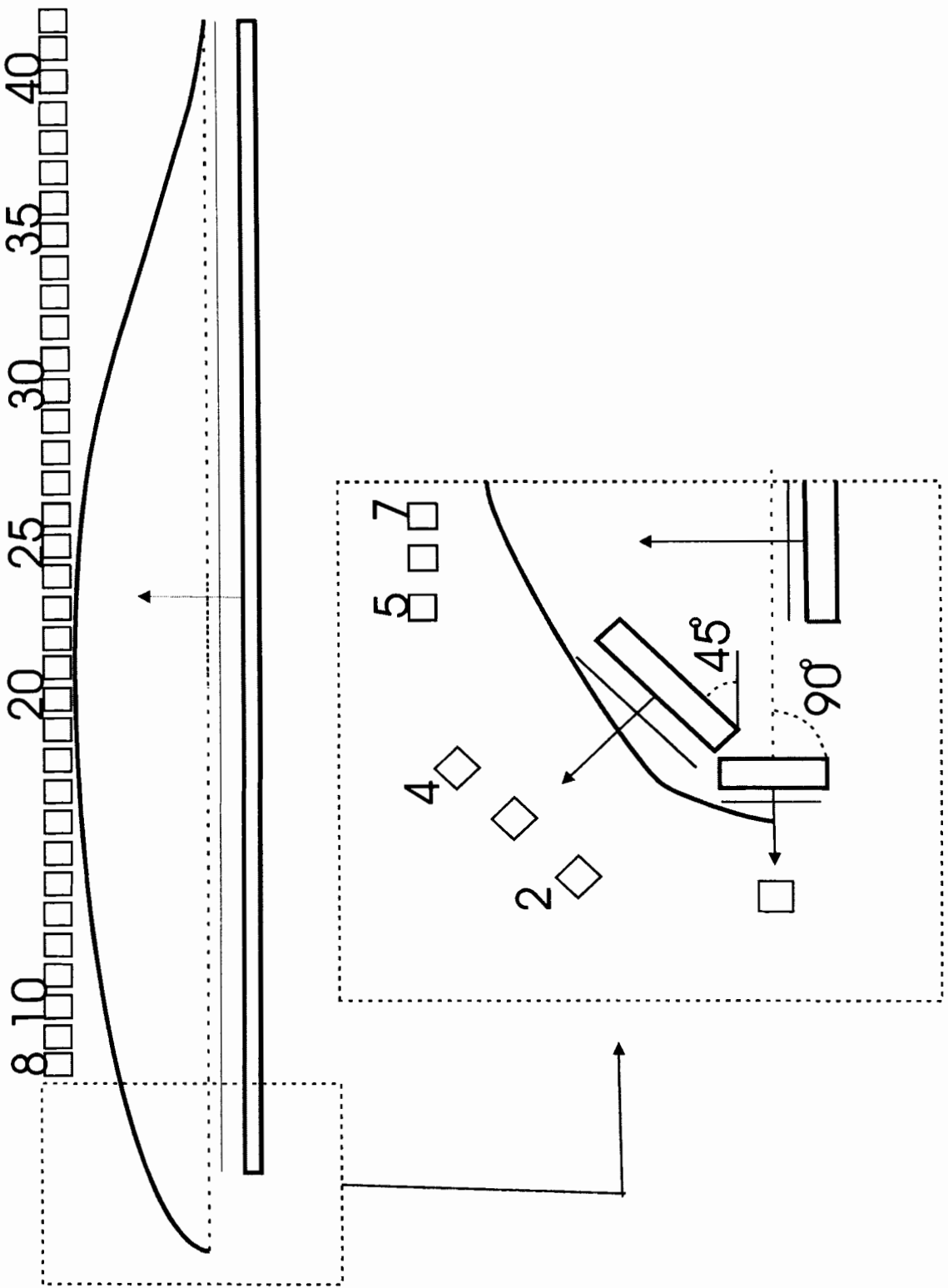
Figure 21: Proposed transducer configuration for reduced-axis scanning system
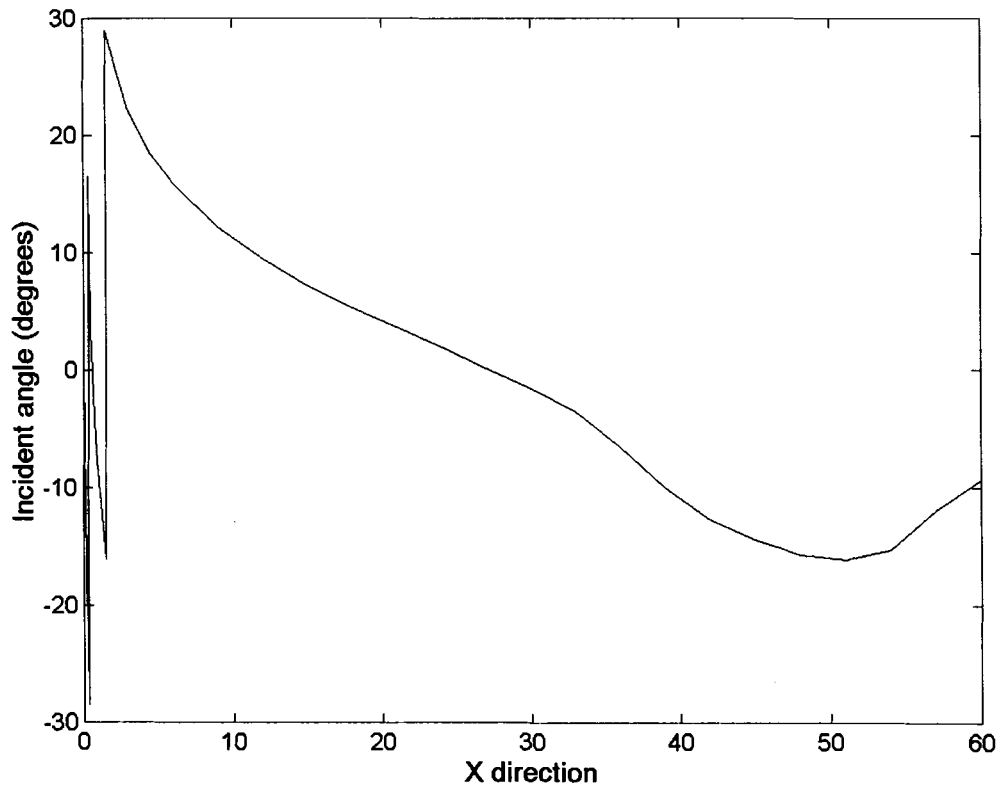
Figure 22: Incident angles for proposed configuration
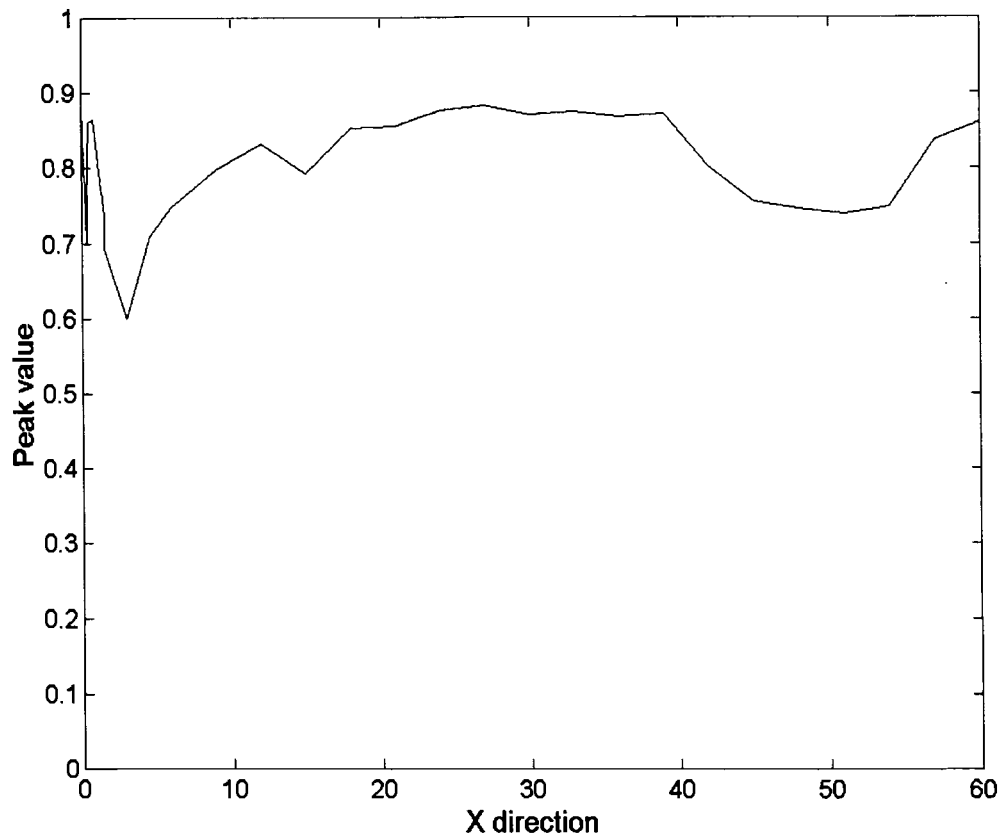
Figure 23: Theoretical peak magnitudes for different points of inspection for $[0, 90]_s$ carbon fiber airfoil

The implementation of the reduced axis scanning algorithm in hardware is key to the practical contribution of the concept. As previously mentioned, the algorithm has been implemented using a compiled Matlab program. However, the calculated values must be implemented in the system hardware. Figure 24 shows the typical through transmission ultrasonic scanning system used in this application. The pulser-receiver (Panametrics 5072PR, Waltham MA) is used to excite a 500 kHz paintbrush transducer (Krautkramer-Bransen, 389-019-710, Lewistown PA). The receiving transducer is a

focused 25 mm. Diameter 500kHz (Panametrics V3895U, Waltham MA). The received signal is amplified by the pulser receiver and sent to an analog peak detector. The DC output of the analog peak detector is in turn sampled by a data acquisition card which has a sample rate determined by the spatial resolution of the scanning system (Microstar Laboratories, DAP-1200a, Bellevue WA). The system differs from most traditional ultrasonic systems since a fixed receiver gain of 20 dB is employed. Gain correction based on the calculated attenuation is employed on the excitation side of the system where a TTL controllable 31.5 dB step attenuator (Alan Industries 50 TTL 31.5) is used on the output of the pulser. This attenuates the input signal to the transducer and can be directly implemented assuming a linear response from the transmitting transducer and other electronics. Control of the step attenuator is performed using the data acquisition card on the ultrasonic system. A large number of digital output lines are available on the data acquisition card and are used to set the value on the step attenuator in this application. The additional cost incurred in this application from the automatic gain is minimal and represents minimal additional complexity when compared to the need for additional axes of motion on the scanning system.
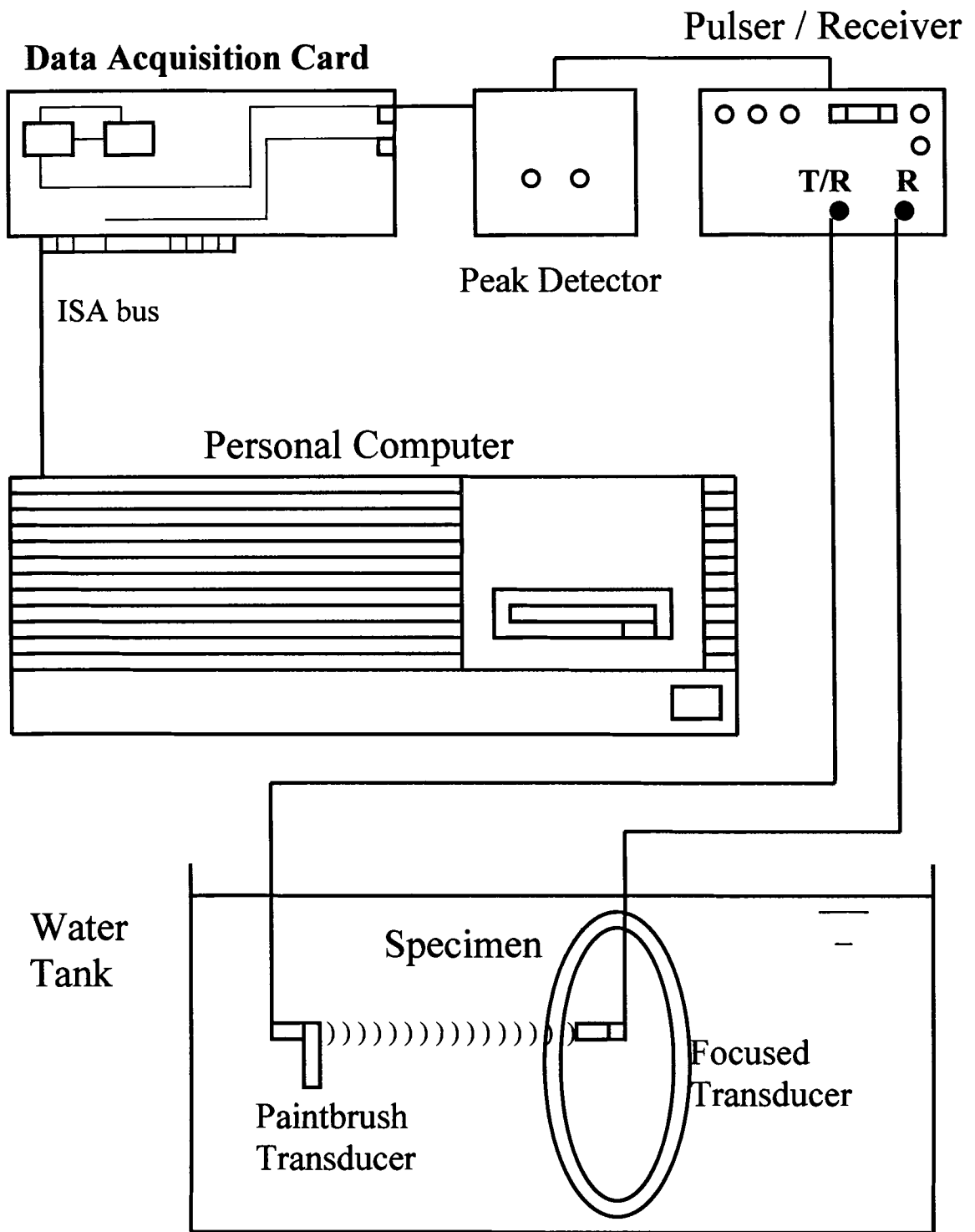
Figure 24: System configuration for scanning airfoil

4. CONCLUSIONS

The focus of this thesis is to enhance the system performance of an ultrasonic scanning machine using mechanics based models and advances in electronics. In this case a model-based gain control to compensate thickness and material variations was developed. Modeling wave propagation interaction with layered media made the calculation of the peak magnitude of the transmitted ultrasonic wave possible. Along with the wave propagation modeling, recent innovations in digital logic technology are applied to enhance system repeatability, a major concern when automating machines. The automatic gain control and improved electronic design, has been shown to have significantly improved the operation of the system.

The robust triggering circuit improved the system repeatability of the ultrasonic scanning machine. The design minimizes the effect of electromagnetic noise in the digital signals from the encoder. Although logic complexity has increased, the number of components and solder connections has also been reduced in the new design. The system demonstrates an application of new logic devices in a complex inspection machine.

The implementation of the model of the wave propagation through layers was shown to be consistent with previous work. The finite transducer bandwidth needed to be accommodated to produce a signal that is comparable to the transmitted signal from a layered material inspection system. Further processing of the standard algorithm was needed. The transmission coefficients were convolved with the transducer response and the finite transducer aperture was considered in a simplified manner. The results from the

52

convolution showed good agreement with the experimental data for the three cases considered. Prior to calculating peak magnitudes, it was shown to be necessary to smooth the transmission coefficient data to remove discontinuities. The need for smoothing results from existence of a finite aperture source and the finite bandwidth of the transducer. A moving average of the angular dependence was used as an alternative to the more computationally expensive approaches that directly account for the effect of the finite aperture source [12].

A practical application for the inspection of an airfoil for a marine science application was also shown to have reasonable agreement. From the description, the hardware implementation of the reduced axis scanning strategy can be implemented at minimal cost using the hardware configuration shown. Using automatic gain correction, the reduced axis scanning system can be applied to other applications of curved panel inspection. Future work needs to consider the effect of visco-elasticity on the absolute signal amplitude, and possibly the peak amplitude variation of the received angle.

The most important contribution to the system is the higher efficiency in the inspection process. Minimal increases in cost and complexity resulted from this work. The potential now exists to increase the number of scan lines in each image without compromising the imaging reliability. An increase in the number of scan-lines results in better image reconstruction, which will allow further work in characterizing the nature of the indications that are detected. The results clearly show the potential for improvement in the system efficiency. The system also minimizes the need for an operator intervention in the work. This will reduce the dependence on the operator for high quality scanning results.

REFERENCES

1. Downs, J., Zhang, P., and Peterson, M. L., "A High-Speed High-Resolution Ultrasonic Inspection Machine", *IEEE/ASME Transactions on Mechatronics* Vol. 4, no. 1, 301-311 (Sept. 1999).

2. Bar-Cohen, Y. and Backes, P. G., "Scanning Aircraft Structures Using Open-Architecture Robotic Crawlers as Platforms with NDT Boards and Sensors", *Materials Evaluation*, (Mar. 1999).

3. Horowitz P., Hill W. *The Art of Electronics*, UK: Cambridge University Press, 1989

4. *Maxim Integrated Products Full-Line Data Catalog*, Maxim Integrated Products, 1999

5. *Foundation Series Quick Start Guide 1. 5* , Xilinx Inc., 1998

6. *The ISP Application Guide and CPLD Data Book*, Xilinx Inc., 1997, p. 3.13

7. Nayfeh, Adnan H., *Wave Propagation in Layered Anisotropic Media*, Elsvier, New York, 173-178 (1995).

8. Krautkramer, J. and Krautkramer, H., *Ultrasonic Testing of Materials*, Springer-Verlag, New York, 182 (1990).

9. Brekhovskikh, L. M. and Godin, O.A., *Acoustics Of Layered Media I*, Springer-Verlag, New York, 98-105 (1990).

10. Nayfeh, Adnan H. and Chimenti, D. E., "Ultrasonic Wave Reflection from Liquid-Coupled Orthotropic Plates with Application to Fibrous Composites", *J. Applied Mechanics*, 55, 863-870 (Dec. 1988).

11. Nayfeh, Adnan H. and Chimenti, D. E., "Elastic Wave Propagation in Fluid-Loaded Multiaxial Anisotropic Media", *J. Acoust. Soc. Am.* 89 (2), 542-549 (1991).

12. Levesque, D. and Piche, L.,"A Robust Transfer Matrix Formulation for the Ultrasonic Response of Multilayered Absorbing Media", *J. Acoust. Soc. Am.* 92 (1), 452-467 (July 1992).

13. Ting, T.C. T., *Anistropic Elasticity: Theory and Applications*, Oxford University Press, New York, 32-39 (1995).

14. Chimenti, D.E. and Nayfeh, Adnan H., "Ultrasonic Reflection and Guided Wave Propagation in Biaxially Laminated Composite Plates", *J. Acoust. Soc. Am.* 87(4), 1409-1415 (1990).

15. Shenghong F. and Radford, D.W., "Elastic Constants of Composites by Measuring Coefficients of Thermal Expansion", submitted to *Composite Materials A*.

16. Proakis, John G. and Manolakis, Dimitris G., *Digital Signal Processing: Principles, Algorithms, and Applications*, Prentice-Hall, New Jersey, 363-364 (1996).

17. Peterson, M. L., "Airfoil Shape Development for Cetacean Biomechanics Research", Report to Composite Materials Manufacturing and Structures Laboratory, Colorado State University, Fort Collins CO, (1999).

APPENDIX:

WAVE PROPAGATION THROUGH ANISOTROPIC

MEDIA

Common Form of the Solution for the Monoclinic Case

For problems involving interfaces, is desirable to cast a formal solution that automatically satisfies the Snell's law requirements, namely that the incident as well as all of the scattered wave components have the same phase at the interface x_3=0 [7].

A formal solution is proposed in the form

$$u_j = U_j e^{i\xi(x_1 + \alpha x_3 - ct)} \qquad\qquad j = 1,2,3, \qquad (1.1)$$

where ξ is the x_1-component of the wave number, c is the common phase velocity ($= \omega/\xi$) along x_1, ω is the circular frequency, α is an unknown ratio of the wave number components along the x_1- and x_3- directions and U_j is the displacement amplitude.

Substituting equation (1.1) into the displacement equations leads to three-coupled equations

$$K_{ij}(\alpha)U_j = 0, \qquad\qquad i,j = 1,2,3, \qquad (1.2)$$

where

$$K_{11} = C_{11} - \rho c^2 + C_{55}\alpha^2$$

$$K_{12} = C_{16} + C_{45}\alpha^2$$

$$K_{13} = \left(C_{13} + C_{55}\right)\alpha$$

$$K_{22} = C_{66} - \rho c^2 + C_{44}\alpha^2$$

$$K_{23} = \left(C_{36} + C_{45}\right)\alpha$$

$$K_{33} = C_{55} - \rho c^2 + C_{33}\alpha^2$$

Analysis

Another way to view the expression (1.2) is

$$\begin{bmatrix} C_{11} - \rho c^2 + C_{55}\alpha^2 & C_{16} + C_{45}\alpha^2 & \left(C_{13} + C_{55}\right)\alpha \\ C_{16} + C_{45}\alpha^2 & C_{66} - \rho c^2 + C_{44}\alpha^2 & \left(C_{36} + C_{45}\right)\alpha \\ \left(C_{13} + C_{55}\right)\alpha & \left(C_{36} + C_{45}\right)\alpha & C_{55} - \rho c^2 + C_{33}\alpha^2 \end{bmatrix} \begin{bmatrix} 1 \\ V \\ W \end{bmatrix} = \begin{bmatrix} 0 \\ 0 \\ 0 \end{bmatrix}$$

where V, W are ratios of the displacement amplitudes of u_2 and u_3 to u_1, respectively. Setting the determinant equal to zero, a sixth-degree polynomial in α is obtain, written as:

$$\alpha^6 + A_1\alpha^4 + A_2\alpha^2 + A_3 = 0 \tag{3}$$

The coefficients are expressed as [10]:

$$A_1 = \left(P_1F_{11} + P_2C_{55} - P_4F_{12} - P_5C_{45} + P_7F_{13}\right)\Big/_{\Delta}$$

$$A_2 = \left(P_2F_{11} + P_3C_{55} - P_5F_{12} - P_6C_{45} + P_8F_{13}\right)\Big/_{\Delta}$$

$$A_3 = \left(P_3F_{11} - P_6F_{12}\right)\Big/_{\Delta}$$

$$\Delta = P_1C_{55} - P_4C_{45}$$

$$P_1 = C_{44}C_{33}; \qquad\qquad P_2 = F_{22}C_{33} + F_{33}C_{44} - F_{23}^2;$$

$$P_3 = F_{22}F_{33}; \qquad\qquad P_4 = C_{33}C_{45};$$

$$P_5 = C_{33}F_{12} + F_{33}C_{45} - F_{13}F_{23}; \qquad\qquad P_6 = F_{12}F_{33};$$

$$P_7 = F_{23}C_{45} + F_{13}C_{44}; \qquad\qquad P_8 = F_{12}F_{23} - F_{13}F_{22};$$

$$F_{11} = C_{11} - \rho c^2; \qquad\qquad F_{12} = C_{16};$$

$$F_{13} = C_{33} + C_{55}; \qquad\qquad F_{22} = C_{66} - \rho c^2;$$

$$F_{23} = C_{36} + C_{45}; \qquad\qquad F_{33} = C_{55} - \rho c^2;$$

Six different solutions are generated form the expression (1.3) for α as

$$\alpha_q, \qquad\qquad q = 1,2...6$$

The displacement component ratios $V_q = {U_{2q}}/{U_{1q}}$ and $W_q = {U_{3q}}/{U_{1q}}$ can

be expressed as:

$$V_q = \frac{K_{11}(\alpha_q)K_{23}(\alpha_q) - K_{13}(\alpha_q)K_{12}(\alpha_q)}{K_{13}(\alpha_q)K_{22}(\alpha_q) + K_{12}(\alpha_q)K_{23}(\alpha_q)} \qquad (1.4)$$

$$W_q = \frac{K_{11}(\alpha_q)K_{23}(\alpha_q) - K_{13}(\alpha_q)K_{12}(\alpha_q)}{K_{12}(\alpha_q)K_{33}(\alpha_q) + K_{23}(\alpha_q)K_{13}(\alpha_q)}.$$ (1.5)

Combining expressions (1.1), (1.4) and (1.5) with the stress-strain relations and using superposition, the formal solutions for each layer for the displacement and stress components can be written as

$$\begin{bmatrix} u_1 & u_2 & u_3 \\ \sigma_{33} & \sigma_{13} & \sigma_{23} \end{bmatrix} = \sum_{q=1}^{6} \begin{bmatrix} 1 & V_q & W_q \\ D_{1q} & D_{2q} & D_{3q} \end{bmatrix} U_q e^{i\xi(x_1 + \alpha_q x - ct)}$$ (1.6)

Suppressing the common factor $e^{i\xi(x_1 - ct)}$ and introducing a change of variable $\sigma_{ij}^* = \sigma_{ij}/i\xi$ for subsequent analyses in the expression (1.6) yields to

$$[u_1 \quad u_2 \quad u_3] = \sum_{q=1}^{6} [1 \quad V_q \quad W_q] U e^{i\xi\alpha_q x_3}$$ (1.7)

$$[\sigma_{33}^* \quad \sigma_{13}^* \quad \sigma_{23}^*] = \sum_{q=1}^{6} [D_{1q} \quad D_{2q} \quad D_{3q}] U e^{i\xi\alpha_q x_3}$$ (1.8)

60

Expressions (1.7) and (1.8) can be combined and written in an expanded matrix

form

$$
\begin{bmatrix} u_1 \\ u_2 \\ u_3 \\ \sigma_{33}^* \\ \sigma_{13}^* \\ \sigma_{23}^* \end{bmatrix} = \begin{bmatrix} 1 & 1 & 1 & 1 & 1 & 1 \\ V_1 & V_2 & V_3 & V_4 & V_5 & V_6 \\ W_1 & W_2 & W_3 & W_4 & W_5 & W_6 \\ D_{11} & D_{12} & D_{13} & D_{14} & D_{15} & D_{16} \\ D_{21} & D_{22} & D_{23} & D_{24} & D_{25} & D_{26} \\ D_{31} & D_{32} & D_{33} & D_{34} & D_{35} & D_{36} \end{bmatrix} \begin{bmatrix} U_{11}E_1 \\ U_{12}E_2 \\ U_{13}E_3 \\ U_{14}E_4 \\ U_{15}E_5 \\ U_{16}E_6 \end{bmatrix}
\qquad (1.9)
$$

where

$$ D_{1q} = C_{13} + C_{36}V_q + C_{33}\alpha_q W_q $$

$$ D_{2q} = C_{55}\left(\alpha_q + W_q\right) + C_{45}\alpha_q V_q $$

$$ D_{3q} = C_{45}\left(\alpha_q + W_q\right) + C_{44}\alpha_q V_q $$

$$ E_q = e^{i\xi\alpha_q x_3} $$

The Local Transfer Matrix

The expression (1.9) can be used to relate the displacements and stresses at $(x'_3)_k = 0$ to those at $(x'_3)_k = d^{(k)}$. The solution can be expressed in a compact form

$$P_k = X_k D_k U_k \qquad (1.10)$$

where

$$X_k = \begin{bmatrix} 1 & 1 & 1 & 1 & 1 & 1 \\ V_1 & V_2 & V_3 & V_4 & V_5 & V_6 \\ W_1 & W_2 & W_3 & W_4 & W_5 & W_6 \\ D_{11} & D_{12} & D_{13} & D_{14} & D_{15} & D_{16} \\ D_{21} & D_{22} & D_{23} & D_{24} & D_{25} & D_{26} \\ D_{31} & D_{32} & D_{33} & D_{34} & D_{35} & D_{36} \end{bmatrix}$$

$$P_k = \begin{bmatrix} u_1 \\ u_2 \\ u_3 \\ \overset{\bullet}{\sigma}_{33} \\ \overset{\bullet}{\sigma}_{13} \\ \overset{\bullet}{\sigma}_{23} \end{bmatrix}_k \qquad \text{is the displacement and stress matrix}$$

$$D_k = \begin{bmatrix} E_1 & 0 & 0 & 0 & 0 & 0 \\ 0 & E_2 & 0 & 0 & 0 & 0 \\ 0 & 0 & E_3 & 0 & 0 & 0 \\ 0 & 0 & 0 & E_4 & 0 & 0 \\ 0 & 0 & 0 & 0 & E_5 & 0 \\ 0 & 0 & 0 & 0 & 0 & E_6 \end{bmatrix}_k$$

$$U_{k=} \begin{bmatrix} U_{11} \\ U_{12} \\ U_{13} \\ U_{14} \\ U_{15} \\ U_{16} \end{bmatrix}_k \quad \text{is the displacement amplitude matrix}$$

Substituting in expression (1.10) for the upper and lower interfaces of the layer k leads to

$$P_k^- = X_k D_k^- U_k \qquad \text{(Upper interface } (x'_3)_k = 0) \qquad (1.11)$$

$$P_k^+ = X_k D_k^+ U_k \qquad \text{(Lower interface } (x'_3)_k = d^{(k)}) \qquad (1.12)$$

$$\text{for } k = 1,2,\ldots,n$$

It is observed that D_k^- results in the identity matrix. Combining the equations (1.11) and (1.12) results in

$$P_k^+ = A_k P_k^- \qquad (1.13)$$

63

where

$$A_k = X_k D_k X_k^{-1} \qquad (1.14)$$

The matrix A_k constitutes the local transfer matrix for the layer k.

The Global Transfer Matrix

Relating the continuity of the displacement and stress components at each layer interface with the local transfer matrix yields to

$$P^+ = A \cdot P^- \qquad (1.15)$$

where

$$A = A_n A_{n-1} \cdots A_1 \qquad (1.16)$$

The matrix A constitutes the global transfer matrix.

Fluid Boundary

The displacements and stresses within the plate-fluid interfaces have to satisfy the continuity conditions

$$\bar{\sigma}_{13} = \bar{\sigma}_{23} = 0, \qquad \bar{\sigma}_{33} = \bar{\sigma}_{33}^{(f)}, \qquad \bar{u}_3 = \bar{u}_3^{(f)}, \qquad \text{at } x_3 = 0 \text{ and } x_3 = d.$$

The continuity conditions for the upper fluid interface can be expressed as

$$\begin{bmatrix} \bar{u}_1 \\ \bar{u}_3 \\ \bar{\sigma}_{33}^{\bullet} \end{bmatrix} = \begin{bmatrix} 1 & 1 \\ \alpha_f & -\alpha_f \\ \rho_f c^2 & \rho_f c^2 \end{bmatrix} \begin{bmatrix} e^{i\xi\alpha_f x_3} \\ R \cdot e^{i\xi\alpha_f x_3} \end{bmatrix} \tag{1.17}$$

The continuity conditions for the lower fluid interface can be written as

$$\begin{bmatrix} \bar{u}_1 \\ \bar{u}_3 \\ \bar{\sigma}_{33}^{\bullet} \end{bmatrix} = \begin{bmatrix} 1 \\ \alpha_f \\ \rho_f c^2 \end{bmatrix} T \cdot e^{i\xi\alpha_f(x_3-d)} \tag{1.18}$$

where

$$\alpha_f^2 = \left(c^2 \Big/ c_f^2 \right) - 1. \tag{1.19}$$

65

Derivation of the Reflection and Transmission Coefficients

Substituting $x_3=0$ and $x_3=d$ in the equations (1.17) and (1.18), respectively, results in

$$\overline{\sigma}_{33}^{*}\bigg|_{x_3=0} = \rho_f c^2 (1+R) \tag{1.20}$$

$$\overline{u}_3\bigg|_{x_3=0} = \alpha_f (1-R) \tag{1.21}$$

$$\overline{\sigma}_{33}^{*}\bigg|_{x_3=d} = \rho_f c^2 T \tag{1.22}$$

$$\overline{u}_3\bigg|_{x_3=0} = \alpha_f T \tag{1.23}$$

The shear stresses vanish in equation (1.15)

$$
\begin{bmatrix} u_1 \\ u_2 \\ u_3 \\ \sigma_{33}^{*} \\ 0 \\ 0 \end{bmatrix}_{x_3=d}
=
\begin{bmatrix}
A_{11} & A_{12} & A_{13} & A_{14} \\
A_{21} & A_{22} & A_{23} & A_{24} \\
A_{31} & A_{32} & A_{33} & A_{34} \\
A_{41} & A_{42} & A_{43} & A_{44} \\
A_{51} & A_{52} & A_{53} & A_{54} \\
A_{61} & A_{62} & A_{63} & A_{64}
\end{bmatrix}
\begin{bmatrix} u_1 \\ u_2 \\ u_3 \\ \sigma_{33}^{*} \end{bmatrix}_{x_3=0}
\tag{1.24}
$$

Substituting the fluid-plate continuity relations, equations (1.20), (1.21), (1.22) and (1.23), in the expression (1.24) yields to

$$
\begin{bmatrix} u_1 \\ u_2 \\ \alpha_f T \\ \rho_f c^2 \cdot T \\ 0 \\ 0 \end{bmatrix}_{x_3=d}
=
\begin{bmatrix} A_{11} & A_{12} & A_{13} & A_{14} \\ A_{21} & A_{22} & A_{23} & A_{24} \\ A_{31} & A_{32} & A_{33} & A_{34} \\ A_{41} & A_{42} & A_{43} & A_{44} \\ A_{51} & A_{52} & A_{53} & A_{54} \\ A_{61} & A_{62} & A_{63} & A_{64} \end{bmatrix}
\begin{bmatrix} u_1 \\ u_2 \\ \alpha_f(1-R) \\ \rho_f c^2(1+R) \end{bmatrix}_{x_3=0}
\qquad (1.25)
$$

Using minor algebraic manipulations in expression (1.25), the reflection and transmission coefficients result in [11]

$$
R = \frac{(M_{21}+Q\cdot M_{22})-Q\cdot(M_{11}+Q\cdot M_{12})}{(M_{21}+Q\cdot M_{22})+Q\cdot(M_{11}+Q\cdot M_{12})}
\qquad (1.26)
$$

$$
T = \frac{2Q\cdot(A_{51}A_{62}-A_{61}A_{52})}{(M_{21}+Q\cdot M_{22})+Q\cdot(M_{11}+Q\cdot M_{12})}
\qquad (1.27)
$$

where

$$
M_{11} = \det \begin{vmatrix} A_{31} & A_{32} & A_{33} \\ A_{51} & A_{52} & A_{53} \\ A_{61} & A_{62} & A_{63} \end{vmatrix}
$$

67

$$M_{12} = \det \begin{vmatrix} A_{31} & A_{32} & A_{34} \\ A_{51} & A_{52} & A_{54} \\ A_{61} & A_{62} & A_{64} \end{vmatrix}$$

$$M_{21} = \det \begin{vmatrix} A_{41} & A_{42} & A_{43} \\ A_{51} & A_{52} & A_{53} \\ A_{61} & A_{62} & A_{63} \end{vmatrix}$$

$$M_{22} = \det \begin{vmatrix} A_{41} & A_{42} & A_{44} \\ A_{51} & A_{52} & A_{54} \\ A_{61} & A_{62} & A_{64} \end{vmatrix}$$

with

$$Q = \frac{\rho_f c^2}{\alpha_f}$$

These are the expressions can be used to calculate the reflection and transmission coefficients for multi-layered plates consisting of an arbitrary number of monoclinic layers immersed in a fluid.

BIOGRAPHY OF THE AUTHOR

Raul Urbina was born in Mexico City, Mexico, on January 08, 1974. After graduation from Colegio Columbia's high school in 1992, he enrolled at the Universidad Panamericana, Mexico City, Mexico, and graduated in 1997 with a Bachelor's degree in Mechanical Engineering. He began his graduate study at The University of Maine in September 1999.

Raul is a candidate for the Master of Science degree in Mechanical Engineering from The University of Maine in May, 2001.